
White Rose Research Online

eprints@whiterose.ac.uk
https://eprints.whiterose.ac.uk
Universities of Leeds, Sheffield and York

Deposited via The University of Sheffield.

White Rose Research Online URL for this paper:
https://eprints.whiterose.ac.uk/id/eprint/98000/

Version: Published Version

Article:
Nolan, P., Kavanagh, C., Dolan, S.R. et al. (2015) Octupolar invariants for compact binaries on quasicircular orbits. Physical Review D (PRD), 92 (12). 123008. ISSN: 1550-7998

https://doi.org/10.1103/PhysRevD.92.123008

Reuse
Items deposited in White Rose Research Online are protected by copyright, with all rights reserved unless indicated otherwise. They may be downloaded and/or printed for private study, or other acts as permitted by national copyright laws. The publisher or other rights holders may allow further reproduction and re-use of the full text version. This is indicated by the licence information on the White Rose Research Online record for the item.

Takedown
If you consider content in White Rose Research Online to be in breach of UK law, please notify us by emailing eprints@whiterose.ac.uk including the URL of the record and the reason for the withdrawal request.



Octupolar invariants for compact binaries on quasicircular orbits

Patrick Nolan,[1] Chris Kavanagh,[1] Sam R. Dolan,[2] Adrian C. Ottewill,[1] Niels Warburton,[3,1] and Barry Wardell[1,4]

[1]*School of Mathematical Sciences and Complex & Adaptive Systems Laboratory, University College Dublin, Belfield, Dublin 4, Ireland*

[2]*Consortium for Fundamental Physics, School of Mathematics and Statistics, University of Sheffield, Hicks Building, Hounsfield Road, Sheffield S3 7RH, United Kingdom*

[3]*MIT Kavli Institute for Astrophysics and Space Research, Massachusetts Institute of Technology, Cambridge, Massachusetts 02139, USA*

[4]*Department of Astronomy, Cornell University, Ithaca, New York 14853, USA*

(Received 13 August 2015; published 23 December 2015)

We extend the gravitational self-force methodology to identify and compute new $\mathcal{O}(\mu)$ tidal invariants for a compact body of mass μ on a quasicircular orbit about a black hole of mass $M \gg \mu$. In the octupolar sector we find seven new degrees of freedom, made up of $3+3$ conservative/dissipative 'electric' invariants and $3+1$ 'magnetic' invariants, satisfying $1+1$ and $1+0$ trace conditions. We express the new invariants for equatorial circular orbits on Kerr spacetime in terms of the regularized metric perturbation and its derivatives; and we evaluate the expressions in the Schwarzschild case. We employ both Lorenz gauge and Regge-Wheeler gauge numerical codes, and the functional series method of Mano, Suzuki and Takasugi. We present (i) highly-accurate numerical data and (ii) high-order analytical post-Newtonian expansions. We demonstrate consistency between numerical and analytical results, and prior work. We explore the application of these invariants in effective one-body models and binary black hole initial-data formulations.

DOI: 10.1103/PhysRevD.92.123008 PACS numbers: 95.30.Sf, 04.20.-q, 04.25.dg

I. INTRODUCTION

The prospect of 'first light' at gravitational wave detectors has spurred much work on the gravitational two-body problem in relativity. It is now a decade since the first (complete) simulations of binary black hole (BH) inspirals and mergers in numerical relativity (NR) [1]. Such simulations have revealed strong-field phenomenology, such as 'superkicks' [2], and have provided template gravitational waveforms. Yet, it may be argued, numerical relativity has also highlighted the 'unreasonable effectiveness' of both post-Newtonian (PN) theory [3], and the effective one-body (EOB) model [4].

BH-BH binaries, and their waveforms, are described by parameters including the masses M, μ, spins, orbital parameters, etc. The parameter space expands for BH-neutron star (NS) binaries—a key target for detection in 2016 [5]—as tidal interactions also play an important role [6,7]. Semianalytic models, such as the EOB model, allow for much finer-grained coverage of parameter space than would be possible with (computationally expensive) NR simulations alone. In addition, effective models can bring physical insight [8–10]. For *real-time* data analysis it may be necessary to blend effective models with surrogate/emulator models [11–13] and careful analysis of modeling uncertainties [14].

By design, the EOB model [15–19] incorporates underdetermined functional relationships, which are 'calibrated' with PN expansions and numerical data. Recently, it was shown that invariant quantities computed via the gravitational self-force (GSF) methodology [20–22] can be used for exactly this purpose [16,23–27]. In fact, as the GSF methodology is designed to provide highly-accurate strong-field data in the extreme mass-ratio regime [28,29], it provides complementary constraints to PN and NR approaches, which excel in the weak-field and comparable mass-ratio regimes, respectively [30]. Thus, new GSF data, nominally limited in scope to the extreme-mass ratio regime, $\mu/M \ll 1$, may immediately be applied to enhance models of comparable-mass inspirals, required for data analysis at, e.g., Advanced LIGO [5].

In recent years, a growing number of invariant quantities, associated with geodesic orbits in black hole spacetimes perturbed through linear order $\mathcal{O}(\mu/M)$, have been extracted from GSF theory. For quasicircular orbits on Schwarzschild, these include (i) the redshift invariant [31,32], (ii) the shift in the innermost stable circular orbit [33], (iii) the periastron advance (of a mildly eccentric orbit) [33,34], (iv) the geodetic spin-precession invariant [26,35,36], (v) tidal eigenvalues [27,37,38], (vi) certain octupolar invariants [27,38]. Recently, (i) has been computed for eccentric orbits [34,39], and (i)–(ii) have been computed for equatorial quasi-circular orbits on Kerr spacetime [40].

In 2008, the GSF redshift invariant at $\mathcal{O}(\mu/M)$ was compared against a post-Newtonian series at 3PN order (i.e., $\mathcal{O}(v^6/c^6)$) [31]. Many further PN expansions have followed for invariants (i)–(vi) at very high PN orders [26,27,35–37,41–43]. An "arms race" between numerical

 © 2015 American Physical Society

(GSF) and analytical (PN) approaches has developed, enabling precise comparisons of high-order coefficients [36,37,41–43]. Such comparisons are invaluable in quality assurance, as they have been used to correct small errors in both GSF calculations [37] and PN expansions [36]. Furthermore, in the "experimental mathematics" approach [41,44], high-order PN coefficients may be extracted in closed (transcendental) form from exquisitely-precise numerical GSF calculations.

The purpose of this paper is to classify and compute GSF invariants at "octupolar" order, i.e., featuring three derivatives of the metric, or equivalently, first derivatives of the Riemann tensor. This sector has been previously considered by Johnson-McDaniel *et al.* [45] and Bini & Damour [27], among others [46–49]. Our intention is to provide a complementary analysis which extends recent GSF work on the dipolar (spin precession) and quadrupolar (tidal) sectors. We aim for completeness, by (i) seeking a complete basis of octupolar invariants, (ii) providing both numerical GSF data and high-order PN expansions at $\mathcal{O}(\mu/M)$.

In outline, the route to obtaining invariants is straightforward: (1) in the GSF formulation, the motion of a small compact body is associated with a geodesic in a *regularly-perturbed vacuum* spacetime [50,51]; (2) the electric tidal tensor $\mathcal{E}_{ab}$ of the regularly-perturbed spacetime defines an orthonormal triad at each point on the geodesic; (3) the covariant derivative of the Riemann tensor $R_{abcd;e}$ resolved in this triad gives a set of well-defined scalar quantities $\{\chi_i\}$; (4) the functional relationships $\chi_i(\Omega)$, where Ω is the circular-orbit frequency, are free of gauge ambiguities; (5) we define the "invariants" $\Delta\chi_i(\Omega)$ to be the $\mathcal{O}(\mu)$ parts of the differences $\chi_i(\Omega,\mu)-\chi_i(\Omega,\mu=0)$.

The article is organized as follows. In Sec. II, we introduce electric and magnetic tidal tensors of octupolar order; decompose in the "electric quadrupole" triad; examine the "background" ($\mu=0$) quantities; and apply perturbation theory to derive invariant quantities through $\mathcal{O}(\mu)$. In Sec. III we describe various computational approaches for obtaining the regular metric perturbation h^R_{ab} and its associated invariants. In Sec. IV we present our results, primarily in the form of tables of data and PN series. In Sec. V we outline two wider applications of our work. We conclude with a discussion of progress and future work in Sec. VI.

Conventions: We set $G=c=1$ and use the metric signature $+2$. In certain contexts where the meaning is clear we also adopt the convention that $M=1$. General coordinate indices are denoted with Roman letters $a,b,c,\ldots$, indices with respect to a triad are denoted with letters $i,j,k,\ldots$, and the index 0 denotes projection onto the tangent vector. The coordinates (t,r,θ,ϕ) denote general polar coordinates which, on the background Kerr spacetime, correspond to Boyer-Lindquist coordinates. Covariant derivatives are denoted using the semi-colon notation, e.g., $k_{a;b}$, with partial derivatives denoted with commas. Symmetrization and antisymmetrization of indices is denoted with round and square brackets, () and [], respectively. Calligraphic tensors (e.g. $\mathcal{E}_{ab}$, $\mathcal{B}_{ab}$) are symmetric in their indices and tracefree.

II. FORMULATION

A. Fundamentals

1. Tidal tensors

We begin by considering a circular-orbit geodesic in the equatorial plane of the regularly-perturbed vacuum Kerr spacetime g_{ab} with a tangent vector u^a. From the Riemann tensor R_{abcd} (equal to the Weyl tensor C_{abcd} in vacuum) we can construct electric-type and magnetic-type "quadrupolar" tensors,

$$\mathcal{E}_{ab}=R_{acbd}u^c u^d, \tag{2.1}$$

$$\mathcal{B}_{ab}=R^*_{acbd}u^c u^d, \tag{2.2}$$

where $R^*_{abcd}=\frac{1}{2}\varepsilon_{ab}{}^{ef}R_{efcd}$. We may also construct "octupolar" tensors,

$$E_{abc}=R_{adbe;c}u^d u^e, \tag{2.3}$$

$$B_{abc}=R^*_{adbe;c}u^d u^e. \tag{2.4}$$

The quadrupolar tensors are symmetric ($\mathcal{E}_{ab}=\mathcal{E}_{ba}$, $\mathcal{B}_{ab}=\mathcal{B}_{ba}$), tracefree ($\mathcal{B}^a{}_a=0$ in general, $\mathcal{E}^a{}_a=0$ in vacuum) and transverse ($\mathcal{E}_{ab}u^b=0=\mathcal{B}_{ab}u^b$). The octupolar tensors are symmetric, and traceless in the first two indices (as $R_{abcd}=R_{cdab}$ and $R_{ab}=R^c{}_{acb}=0$) in vacuum. By contracting the Bianchi identity (or its dual) $R_{abcd;e}+R_{abde;c}+R_{abec;d}=0$, we observe that the octupolar tensors are also traceless on the latter pair of indices, $E_{ab}{}^b=0=B_{ab}{}^b$, in vacuum. Note however that the octupolar tensors are *not* symmetric in the latter pair of indices, in general.

2. Tetrad components

Let us now introduce an orthonormal tetrad $\{e^a_0=u^a,e^a_i\}$ on the worldline and define tetrad-resolved quantities in the natural way, so that

$$\chi_{i0j\ldots}=\chi_{abc\ldots}e^a_i u^b e^c_j\ldots, \tag{2.5}$$

where $\chi_{abc\ldots}$ is any tensor and $i,j,k\in\{1,2,3\}$. The quadrupole components are spatial, $\mathcal{E}_{00}=\mathcal{E}_{0i}=0=\mathcal{B}_{0i}=\mathcal{B}_{00}$. The octupole components are spatial in first two indices, but not in general. We may then consider three types of electric octupolar terms, namely,

$$E_{ij0}, E_{i[jk]}, \quad \text{and} \quad \mathcal{E}_{ijk} \equiv E_{(ijk)}, \tag{2.6}$$

and similarly in the magnetic sector.

Note that $\mathcal{E}_{ij}$ is real and symmetric, and thus its eigenvalues are real and its eigenvectors are orthogonal. Thus, we may select our triad e^i_a to coincide with the electric-quadrupolar eigenbasis. In other words, we choose the triad in which $\mathcal{E}_{ij}$ is diagonal. We choose e^a_2 to be the vector orthogonal to the equatorial plane.

3. Equatorial symmetry

For circular equatorial orbits, the reflection-in-equatorial plane symmetry implies that many components are identically zero. Namely,

$$\mathcal{E}_{12} = \mathcal{E}_{23} = \mathcal{B}_{11} = \mathcal{B}_{13} = \mathcal{B}_{22} = \mathcal{B}_{33} = 0, \tag{2.7}$$

$$E_{112} = E_{222} = E_{233} = E_{123} = 0, \tag{2.8}$$

$$B_{111} = B_{122} = B_{133} = B_{113} = B_{223} = B_{333} = 0, \tag{2.9}$$

with all permutations of these indices also zero.

B. Classification of octupolar components

Now we consider the three types of terms (2.6) separately, and show that E_{ij0}, B_{ij0} and $E_{i[jk]}$, $B_{i[jk]}$ may be derived from dipolar and quadrupolar terms, whereas $\mathcal{E}_{ijk} \equiv E_{(ijk)}$, $\mathcal{B}_{ijk} \equiv B_{(ijk)}$ encode new information at octupolar order.

1. E_{ij0} and B_{ij0}

For circular orbits, we have $u^b e^a_{1;b} = \omega e^a_3$, $u^b e^a_{2;b} = 0$ and $u^b e^a_{3;b} = -\omega e^a_1$, where ω is the precession frequency with respect to proper time, defined by parallel transport observed from the electric eigenbasis (cf. Refs. [35,37]). As the quadrupolar eigenvalues are time-independent on circular orbits, the only nontrivial components are

$$E_{130} = \omega(E_{11} - E_{33}), \qquad B_{120} = -\omega B_{23},$$
$$B_{230} = \omega B_{12}. \tag{2.10}$$

2. $E_{i[jk]}$ and $B_{i[jk]}$

By virtue of the Bianchi identity,

$$E_{a[bc]} = -\frac{1}{2} u^e (u^d R_{dabc})_{;e}, \qquad B_{a[bc]} = -\frac{1}{2} u^e (u^d R^*_{dabc})_{;e}. \tag{2.11}$$

We now (i) project onto the tetrad, (ii) use that $\mathcal{B}_{ij} = \frac{1}{2}\epsilon_{jkl} R_{0ikl}$ and $\mathcal{E}_{ij} = -\frac{1}{2}\epsilon_{jkl} R^*_{0ikl}$, and (iii) recall that the tetrad components in the electric frame are constants for circular orbits. Thus all components are zero except

$$E_{2[23]} = E_{1[31]} = \frac{1}{2}\omega \mathcal{B}_{23}, \tag{2.12}$$

$$E_{3[31]} = E_{2[12]} = -\frac{1}{2}\omega \mathcal{B}_{12}, \tag{2.13}$$

$$B_{1[12]} = B_{3[23]} = \frac{1}{2}\omega(\mathcal{E}_{11} - \mathcal{E}_{33}), \tag{2.14}$$

and permutations thereof.

3. $\mathcal{E}_{ijk}$ and $\mathcal{B}_{ijk}$

In general, $\mathcal{E}_{ijk}$ and $\mathcal{B}_{ijk}$ each have ten components satisfying 3 trace conditions, i.e., seven independent components each. For circular orbits, 4 electric and 6 magnetic components are zero, respectively, leaving 6 and 4 nontrivial quantities satisfying 2 and 1 nontrivial trace conditions. In other words, there are 10 quantities we may calculate (given below), satisfying 3 nontrivial trace conditions; thus, 7 new independent degrees of freedom at octupolar order.

4. Additional invariants

Other octupolar quantities may be written in terms of the set identified above. For example, a relevant quantity in EOB theory [see Ref. [27], Eq. (D10)] is $K_{3+} \equiv \mathcal{E}_{abc}\mathcal{E}^{abc}$, which may be expressed as

$$K_{3+} = \mathcal{E}^2_{111} + \mathcal{E}^2_{333} + 3(\mathcal{E}^2_{122} + \mathcal{E}^2_{133} + \mathcal{E}^2_{311} + \mathcal{E}^2_{322}) - 6\mathcal{E}^2_{130}, \tag{2.15}$$

where $\mathcal{E}_{130} = \frac{1}{3}E_{130}$.

C. Circular orbits: Background quantities

Below we give the values of the tidal quantities for circular equatorial geodesics on the unperturbed Kerr spacetime, i.e., for test-masses ($\mu = 0$). Here, the orbital radius is r_0 and the orbital frequency is $\Omega = \sqrt{M}/(r_0^{3/2} + a\sqrt{M})$ where a is the Kerr spin parameter and $a > 0$ ($a < 0$) for prograde (retrograde) orbits.

The tangent vector u^a and electric-eigenbasis triad have the components [52]

$$u^a = [U, 0, 0, \Omega U], \tag{2.16a}$$

$$e^a_1 = [0, \sqrt{\Delta_0}/r_0, 0, 0], \tag{2.16b}$$

$$e^a_2 = [0, 0, 1/r_0, 0], \tag{2.16c}$$

$$e^a_3 = -\epsilon^a{}_{bcd} u^b e^c_1 e^d_2, \tag{2.16d}$$

where $U = \sqrt{M}/(\Omega r_0^{3/2} v)$, $\Delta_0 = r_0^2 - 2Mr_0 + a^2$ and

$$v^2 \equiv 1 - 3M/r_0 + 2a\sqrt{M}/r_0^{3/2}. \tag{2.17}$$

The spin precession rate is $\omega = \sqrt{Mr_0}/r_0^2$.

1. Quadrupolar components

The (nontrivial) quadrupolar components are

$$\mathcal{E}_{11} = \frac{M}{r_0^3} - \frac{3M\Delta_0}{v^2 r_0^5}, \tag{2.18a}$$

$$\mathcal{E}_{22} = -\frac{2M}{r_0^3} + \frac{3M\Delta_0}{v^2 r_0^5}, \tag{2.18b}$$

$$\mathcal{E}_{33} = \frac{M}{r_0^3}, \tag{2.18c}$$

$$\mathcal{B}_{12} = -\frac{3M^{3/2}\sqrt{\Delta_0}(1 - a/\sqrt{Mr_0})}{r_0^{9/2}v^2}, \tag{2.18d}$$

We note that $\mathcal{B}_{23} = 0$ on the background.

2. Octupolar components

In the electric sector,

$$\mathcal{E}_{111} = +\mathcal{A}(6r_0^2 - 9Mr_0 - 12a\sqrt{Mr_0} + 15a^2) \tag{2.19}$$

$$\mathcal{E}_{122} = -\mathcal{A}(3r_0^2 - 2Mr_0 - 16a\sqrt{Mr_0} + 15a^2) \tag{2.20}$$

$$\mathcal{E}_{133} = -\mathcal{A}(3r_0^2 - 7Mr_0 + 4a\sqrt{Mr_0}), \tag{2.21}$$

where $\mathcal{A} = \sqrt{\Delta_0}M/(r_0^7 v^2)$. We note that $\mathcal{E}_{311} = \mathcal{E}_{322} = \mathcal{E}_{333} = 0$ on the Kerr background.

In the magnetic sector,

$$\begin{aligned}\mathcal{B}_{211} = &+\mathcal{C}(4r_0^2 - 8Mr_0 + 7a^2) \\ &- \mathcal{D}(4r_0^2 - 7Mr_0 + 5a^2),\end{aligned} \tag{2.22}$$

$$\begin{aligned}\mathcal{B}_{222} = &-\mathcal{C}(3r_0^2 - 6Mr_0 + 9a^2) \\ &+ \mathcal{D}(3r_0^2 - 4Mr_0 + 5a^2),\end{aligned} \tag{2.23}$$

$$\begin{aligned}\mathcal{B}_{233} = &-\mathcal{C}(r_0^2 - 2Mr_0 - 2a^2) \\ &+ \mathcal{D}(r_0^2 - 3Mr_0),\end{aligned} \tag{2.24}$$

where $\mathcal{C} = 2M^{3/2}/(r_0^{13/2}v^2)$ and $\mathcal{D} = 3aM/(r_0^7 v^2)$. Note that $\mathcal{B}_{123} = 0$ on the Kerr background.

The "derived" quantities E_{ij0}, $E_{i[jk]}$, etc., may be easily calculated using Eq. (2.10), Eq. (2.12)–(2.14) and Eq. (2.19)–(2.24). For example, in the Schwarzschild ($a = 0$) case, using Eq. (2.15) yields

$$K_{3+} = \frac{6M^2(1 - 2M/r_0)(15r_0^2 - 46Mr_0 + 42M^2)}{r_0^{10}(1 - 3M/r_0)^2}. \tag{2.25}$$

D. Circular orbits: Perturbation theory

Here we seek expressions for the octupolar quantities in the regular perturbed spacetime $\bar{g}_{ab} + h^R_{ab}$, where $\bar{g}_{ab}$ is the Kerr metric in Boyer-Lindquist coordinates, and $h^R_{ab} = \mathcal{O}(\mu)$ is the "regular" metric perturbation defined by Detweiler and Whiting [50]. We work to first order in the small mass μ, neglecting all terms at $\mathcal{O}(\mu^2)$, and noting that the regular perturbed spacetime is Ricci-flat.

We take the standard two-step approach [31,32,37]. For a given geodesic quantity χ (e.g. $\mathcal{E}_{111}$), we first compare χ on a circular geodesic in the perturbed spacetime with χ on a circular geodesic of the background spacetime at the same coordinate radius $r = r_0$. Then, noting that r_0 itself varies under a gauge transformation at $\mathcal{O}(\mu)$, we apply a correction to compare χ on two geodesics which share the same orbital frequency Ω.

Following the convention of Ref. [37], we use an "overbar" to denote "background" quantities, so that barred quantities such as $\bar{u}^a$ are assigned the same coordinate values as in Sec. II C. We use δ to denote the difference at $\mathcal{O}(\mu)$, i.e., $\delta e^a_i \equiv e^a_i - \bar{e}^a_i$. At $\mathcal{O}(\mu)$, δ may be applied as an operator with a Leibniz rule $\delta(AB) = (\delta A)B + A\delta B$. In general, such differences are gauge-dependent. To obtain an invariant difference, we introduce the "frequency-radius" r_Ω via

$$\Omega = \sqrt{M}/(r_\Omega^{3/2} + a\sqrt{M}). \tag{2.26}$$

Then, we write

$$\chi(r_\Omega) - \bar{\chi}(r_\Omega) = \Delta\chi(r_0) + \mathcal{O}(\mu^2). \tag{2.27}$$

Here $\bar{\chi}(r_\Omega)$ has the same functional form as χ on the background spacetime, with r_0 replaced by r_Ω. As $\Delta\chi$ is at $\mathcal{O}(\mu)$, we may parametrize $\Delta\chi$ using the $\mathcal{O}(\mu^0)$ background radius r_0, rather than r_Ω, as $r_0 - r_\Omega = \mathcal{O}(\mu)$. Such relationships, $\Delta\chi(r_0)$, are invariant within the class of gauges in which the metric perturbation is helically symmetric (implying that $\bar{u}^c h^R_{ab,c} = 0$ at the relevant order).

1. Perturbation of the tetrad

We may write the variation of the tetrad legs in the following way,

$$\delta u^a = \beta_{00}\bar{u}^a + \beta_{03}\bar{e}^a_3, \tag{2.28a}$$

$$\delta e^a_i = \beta_{i0}\bar{u}^a + \sum_{j=1}^{3}\beta_{ij}\bar{e}^a_j. \tag{2.28b}$$

with the coefficients $\beta_{ab} = \mathcal{O}(\mu)$ to be determined below. First, we note that β_{00} and β_{03} may be found by recalling key relations previously established in GSF theory for equatorial circular orbits on Kerr spacetime [31,53], namely,

$$\frac{\delta u^t}{\bar{u}^t} = \frac{1}{2}h_{00} - \frac{\bar{\Omega}}{2}\sqrt{\frac{r_0}{M}}(r_0^2 + a^2 - 2a\sqrt{Mr_0})\tilde{F}_r, \quad (2.29)$$

$$\frac{\delta u^\phi}{\bar{u}^\phi} = \frac{1}{2}h_{00} - \frac{1}{2M}(r_0^2 - 2Mr_0 + a\sqrt{Mr_0})\tilde{F}_r. \quad (2.30)$$

Here $h_{00} \equiv h^R_{ab}\bar{u}^a\bar{u}^b$, and $\tilde{F}_r \equiv \mu^{-1}F_r = \mathcal{O}(\mu)$ is the (specific) radial self-force given by

$$\tilde{F}_r = \frac{1}{2}\bar{u}^a\bar{u}^b\frac{\partial h^R_{ab}}{\partial r}\bigg|_{r=r_0}. \quad (2.31)$$

Hence we have $\beta_{00} = \frac{1}{2}h_{00}$ and $\beta_{03} = -\frac{1}{2}\sqrt{\frac{r_0\Delta_0}{M}}\tilde{F}_r$. The diagonal coefficients β_{ii} follow from the normalization condition, $(\bar{g}_{ab} + h^R_{ab})(\bar{e}^a_i + \delta e^a_i)(\bar{e}^b_j + \delta e^b_j) = \delta_{ij}$. That is, $\beta_{ii} = -\frac{1}{2}h_{ii}$, where $h_{ii} = h^R_{ab}\bar{e}^a_i\bar{e}^b_i$ (no summation over i implied). From orthogonality of legs 0 and 3, we have $\beta_{30} = \beta_{03} + h_{03}$ where $h_{03} = h^R_{ab}\bar{u}^a\bar{e}^b_3$. By similar reasoning, $\beta_{10} = h_{01}$ and $\beta_{31} + \beta_{13} + h_{13} = 0$. To eliminate the residual rotational freedom in the triad at $\mathcal{O}(\mu)$, we now impose the condition that the triad is aligned with the electric eigenbasis, i.e., that $\mathcal{E}_{ij}$ is diagonal in the perturbed spacetime (so that, e.g., $\mathcal{E}_{13} = 0$). From this condition it follows that

$$\beta_{13} = \frac{(\delta R)_{1030} - \bar{\mathcal{E}}_{11}h_{13}}{\bar{\mathcal{E}}_{11} - \bar{\mathcal{E}}_{33}}, \quad (2.32)$$

$$\beta_{31} = \frac{-(\delta R)_{1030} + \bar{\mathcal{E}}_{33}h_{13}}{\bar{\mathcal{E}}_{11} - \bar{\mathcal{E}}_{33}}, \quad (2.33)$$

where

$$(\delta R)_{1030} = \delta R_{abcd}\bar{e}^a_1\bar{u}^b\bar{e}^c_3\bar{u}^d. \quad (2.34)$$

2. Perturbation of octupolar components

Here we present results for the perturbation of the (symmetric tracefree) octupolar components $\mathcal{E}_{ijk}$ and $\mathcal{B}_{ijk}$. The electric components are

$$\delta\mathcal{E}_{111} = (\delta\nabla R)_{(10101)} + \left(h_{00} - \frac{3}{2}h_{11}\right)\bar{\mathcal{E}}_{111} + 2\beta_{03}\bar{\mathcal{R}}_{10131}, \quad (2.35a)$$

$$\delta\mathcal{E}_{122} = (\delta\nabla R)_{(10202)} + \left(h_{00} - \frac{1}{2}h_{11} - h_{22}\right)\bar{\mathcal{E}}_{122} + 2\beta_{03}\bar{\mathcal{R}}_{10232}, \quad (2.35b)$$

$$\delta\mathcal{E}_{133} = (\delta\nabla R)_{(10303)} + \left(h_{00} - \frac{1}{2}h_{11} - h_{33}\right)\bar{\mathcal{E}}_{133} + 2\beta_{03}\bar{\mathcal{R}}_{10333} + \frac{2}{3}\beta_{30}\bar{\omega}(\bar{\mathcal{E}}_{11} - \bar{\mathcal{E}}_{33}), \quad (2.35c)$$

$$\delta\mathcal{E}_{113} = (\delta\nabla R)_{(10103)} + \frac{2}{3}\beta_{10}\bar{\omega}(\bar{\mathcal{E}}_{11} - \bar{\mathcal{E}}_{33}) + \beta_{31}\bar{\mathcal{E}}_{111} + 2\beta_{13}\bar{\mathcal{E}}_{133}, \quad (2.35d)$$

$$\delta\mathcal{E}_{223} = (\delta\nabla R)_{(20203)} + \beta_{31}\bar{\mathcal{E}}_{122}, \quad (2.35e)$$

$$\delta\mathcal{E}_{333} = (\delta\nabla R)_{(30303)} + 3\beta_{31}\bar{\mathcal{E}}_{133}, \quad (2.35f)$$

where

$$(\delta\nabla R)_{(i0j0k)} = \delta R_{abcd;e}\bar{u}^b\bar{u}^d\bar{e}^{(a}_i\bar{e}^c_j\bar{e}^{e)}_k, \quad (2.36)$$

$$\bar{\mathcal{R}}_{i0j3k} = \bar{R}_{abcd;e}\bar{u}^{(b}\bar{e}^{d)}_3\bar{e}^{(a}_i\bar{e}^c_j\bar{e}^{e)}_k. \quad (2.37)$$

The magnetic components are

$$(\delta\mathcal{B})_{211} = (\delta\nabla R^*)_{20101} + \left(h_{00} - h_{11} - \frac{1}{2}h_{22}\right)\bar{\mathcal{B}}_{211} + 2\beta_{03}\bar{\mathcal{R}}^*_{20131}, \quad (2.38a)$$

$$(\delta\mathcal{B})_{222} = (\delta\nabla R^*)_{20202} + \left(h_{00} - \frac{3}{2}h_{22}\right)\bar{\mathcal{B}}_{222} + 2\beta_{03}\bar{\mathcal{R}}^*_{20232}, \tag{2.38b}$$

$$(\delta\mathcal{B})_{233} = (\delta\nabla R^*)_{20303} + \left(h_{00} - \frac{1}{2}h_{22} - h_{33}\right)\bar{\mathcal{B}}_{233} + 2\beta_{03}\bar{\mathcal{R}}^*_{20333} + \frac{2}{3}\beta_{30}\bar{\omega}\bar{\mathcal{B}}_{12}, \tag{2.38c}$$

$$(\delta\mathcal{B})_{123} = (\delta\nabla R^*)_{10203} + \beta_{13}\bar{\mathcal{B}}_{233} + \beta_{31}\bar{\mathcal{B}}_{211} + \frac{1}{3}\beta_{10}\bar{\omega}\bar{\mathcal{B}}_{12}, \tag{2.38d}$$

where

$$(\delta\nabla R^*)_{(i0j0k)} = \delta R^*_{abcd;e}\bar{u}^b\bar{u}^d\bar{e}_i^{(a}\bar{e}_j^c\bar{e}_k^{e)}, \tag{2.39}$$

$$\bar{\mathcal{R}}^*_{i0j3k} = \bar{R}^*_{abcd;e}\bar{u}^{(b}\bar{e}_3^{d)}\bar{e}_i^{(a}\bar{e}_j^c\bar{e}_k^{e)}. \tag{2.40}$$

3. Invariant relations

As noted above, the coordinate radius of the orbit, $r = r_0$, is not invariant under changes of gauge [i.e., coordinate changes at $\mathcal{O}(\mu)$]. On the other hand, the orbital frequency Ω is invariant under helically symmetric gauge transformations. Following Eq. (2.27), we may therefore express the functional relationship between $\chi \in \{\mathcal{E}_{111}, \ldots\}$ and Ω as follows,

$$\chi(r_\Omega) = \bar{\chi}(r_\Omega) + \Delta\chi(r_0) + \mathcal{O}(\mu^2), \tag{2.41}$$

where r_Ω is the frequency-radius defined in Eq. (2.26), and $\Delta\chi = \mathcal{O}(\mu)$. Note that $\bar{\chi}(r_\Omega)$ denotes the "test-particle" functions defined in Sec. II C evaluated at r_Ω. By definition, we have $\Delta\Omega = 0$. At $\mathcal{O}(\mu)$,

$$\Delta\chi = \delta\chi - \delta\Omega\frac{dr_0}{d\bar{\Omega}}\frac{d\bar{\chi}}{dr_0}, \tag{2.42}$$

or, making use of Eq. (2.29) and (2.30) and $\delta\Omega/\bar{\Omega} = \delta u^\phi/\bar{u}^\phi - \delta u^t/\bar{u}^t$,

$$\Delta\chi = \delta\chi - \frac{1}{3M}r_0^3 v^2 \tilde{F}_r\frac{d\bar{\chi}}{dr_0}. \tag{2.43}$$

In summary, $\Delta\chi$ defined by Eq. (2.43), Eq. (2.35) and Eq. (2.38) are the invariant quantities which we will compute in the next sections.

4. Further quantities

In Sec. II B we wrote E_{ij0}, $E_{i[jk]}$, B_{ij0}, $B_{i[jk]}$ in terms of quadrupolar tidal components, and the spin precession scalar ω. If required, one may deduce the variation of these components by applying Δ as a Leibniz operator. For example, starting with Eq. (2.10),

$$\Delta\mathcal{E}_{130} = \Delta\omega(\bar{\mathcal{E}}_{11} - \bar{\mathcal{E}}_{33}) + \bar{\omega}(\Delta\mathcal{E}_{11} - \Delta\mathcal{E}_{33}). \tag{2.44}$$

Numerical data for the variation in the quadrupolar components $\Delta\mathcal{E}_{11}, \ldots, \Delta\mathcal{B}_{21}, \ldots$ is given in Table I of Ref. [37]. We may compute $\Delta\omega$ from the redshift and spin-precession invariants, ΔU and $\Delta\psi$, using

$$\Delta\omega = \frac{\bar{\omega}}{\bar{U}}\Delta U - \bar{U}\,\bar{\Omega}\,\Delta\psi, \tag{2.45}$$

together with the data in Table III of Ref. [37].

Similarly, the variation ΔK_{3+}, for example, can be found by applying Δ in this manner to Eq. (2.15). This can then be related to the quantity $\hat{\delta}_{K3+}$, whose post-Newtonian expansion was given to 7.5PN in Ref. [27]. Noting that $K_{3+} \equiv \Gamma^4\mathcal{K}_{3+}$ and

$$\Gamma = \frac{1}{\sqrt{1-3M/r_0}}\left[1 + \frac{1}{2}h_{00} + \mathcal{O}(\mu^2)\right], \tag{2.46}$$

we then have a relation between the first-order perturbations,

$$\frac{\Delta K_{3+}}{\bar{K}_{3+}} = \hat{\delta}_{K3+} + 2h_{00}. \tag{2.47}$$

III. COMPUTATIONAL APPROACHES

In this section we outline our methods for computing the octupolar invariants for a particle of mass μ on a circular orbit of radius r_0 in Schwarzschild geometry. Our approaches break into two broad categories: (i) numerical integration of the linearized Einstein equation in either the Regge-Wheeler (RW) or Lorenz gauge and (ii) analytically solving the Regge-Wheeler field equations as a series of special functions via the Mano-Suzuki-Takasugi (MST) method. In both cases we decompose the linearized Einstein equation into tensor-harmonic and Fourier modes and solve for the resulting decoupled radial equation. In this section, and subsections that follow, l and m are the tensor-harmonic multipole indices, ω is the mode frequency and we work with standard Schwarzschild coordinates (t, r, θ, φ). For this section let us also define $f \equiv f(r) = 1 - 2M/r$. We shall also use a subscript "0" to denote a quantity evaluated at the particle. Finally, note that for a circular orbit about a Schwarzschild black hole the particle's (specific) orbital energy and angular-momentum are given by

$$\mathbb{E}_0 = \frac{r_0 - 2M}{\sqrt{r_0(r_0 - 3M)}}, \qquad \mathbb{L}_0 = r_0\sqrt{\frac{M}{r_0 - 3M}}, \tag{3.1}$$

respectively.

For calculations in the RW gauge there is a single "master" radial function, $\Psi_{lm\omega}$, to be solved for each tensor-harmonic and Fourier mode [54,55]. For circular orbits the Fourier spectrum is discrete and given by $\omega \equiv \omega_m = m\Omega$ where $\Omega = \sqrt{M/r_0^3}$ is the azimuthal orbital frequency. Consequently, we label the RW master function with only lm subscripts hereafter. The full metric perturbation can be rebuilt from the Ψ_{lm}'s and their derivatives [56]. For $l \geq 2$ the ordinary differential equation that Ψ_{lm} obeys takes the form

$$\left(\frac{d^2}{dr_*^2} + [\omega_m^2 - U_l(r)]\right)\Psi_{lm} = \mathcal{S}_1\delta(r - r_0) + \mathcal{S}_2\delta'(r - r_0), \tag{3.2}$$

where r_* is the radial "tortoise" coordinate given by $dr_*/dr = f^{-1}$ and $U(r)$ is an effective potential. The effective potential used depends on whether the perturbation is odd or even parity. For the odd/even parity modes, equivalently $l + m = \text{odd/even}$, the potential is given by

$$U_l^o(r) = \frac{f}{r^2}\left(l(l+1) - \frac{6M}{r}\right), \tag{3.3}$$

$$U_l^e(r) = \frac{f}{r^2\Lambda^2}\left[2\lambda^2\left(\lambda + 1 + \frac{3M}{r}\right) + \frac{18M^2}{r^2}\left(\lambda + \frac{M}{r}\right)\right], \tag{3.4}$$

respectively, where $\lambda = (l+2)(l-1)/2$ and $\Lambda = \lambda + 3M/r_0$. The form of the source terms, $\mathcal{S}_i$, also differs for the even and odd sectors. Explicitly, the odd sector sources take the form [57]

$$\mathcal{S}_1^o = -\frac{2pf_0\mathcal{L}_0}{\lambda l(l+1)}X_\phi^*(\theta,\phi), \tag{3.5}$$

$$\mathcal{S}_2^o = \frac{2pr_0f_0^2\mathcal{L}_0}{\lambda l(l+1)}X_\phi^*(\theta,\phi). \tag{3.6}$$

For the even sector, we have

$$\mathcal{S}_1^e = \frac{pq\mathcal{E}_0}{r_0f_0\Lambda}\left[\frac{\mathcal{L}_0^2}{\mathcal{E}_0^2}f_0^2\Lambda - (\lambda(\lambda+1)r_0^2 + 6\lambda Mr_0 + 15M^2)\right]Y_{lm}^*(\theta,\phi) - \frac{4p\mathcal{L}_0^2f_0^2}{r_0\mathcal{E}_0}\frac{(l-2)!}{(l+2)!}Y_{\phi\phi}^*(\theta,\phi), \tag{3.7}$$

$$\mathcal{S}_2^e = (r_0^2pq\mathcal{E}_0)Y_{lm}^*(\theta,\phi), \tag{3.8}$$

where we have defined the following expressions for convenience:

$$X_\phi(\theta,\phi) = \sin\theta\partial_\theta Y_{lm}(\theta,\phi), \tag{3.9}$$

$$Y_{\phi\phi}(\theta,\phi) = \left(\partial_{\phi\phi} + \sin\theta\cos\theta\partial_\theta + \frac{l(l+1)}{2}\sin^2\theta\right) \times Y_{lm}(\theta,\phi) \tag{3.10}$$

$$p = \frac{8\pi\mu}{r_0^2}, \qquad q = \frac{f_0^2}{(\lambda+1)\Lambda}. \tag{3.11}$$

For the radiative modes $l \geq 2$, $m \neq 0$ we will construct homogeneous solutions to Eq. (3.2) either numerically or as a series of special functions, as outlined in the subsections below. For the static ($l \geq 2$, $m = 0$) modes, closed-form analytic solutions to the homogeneous RW equation are known. In the odd sector these can be written in terms of standard hypergeometric functions:

$$\tilde{\Psi}_{l0}^{o-} = x^{-l-1}{}_2F_1(-l-2, -l+2, -2l, x) \tag{3.12}$$

$$\tilde{\Psi}_{l0}^{o+} = x^l{}_2F_1(l-1, l+3, 2+2l, x), \tag{3.13}$$

where hereafter an overtilde denotes a homogeneous solution, a "+" superscript denotes an outer solution (regular at spatial infinity, divergent at the horizon), a "−" denotes an inner solution (regular at the horizon, divergent at spatial infinity) and $x = 2M/r$. In practice, we need only solve the simpler odd sector field equations, and construct the even sector homogeneous solutions via the transformation [56]:

$$\tilde{\Psi}_{lm}^{e\pm} = \frac{1}{\lambda + \lambda^2 \pm 3i\omega M}\left[\left(\lambda + \lambda^2 + \frac{9M^2(r-2M)}{r^2(r\lambda + 3M)}\right)\tilde{\Psi}_{lm}^{o\pm} + 3Mf\frac{d\tilde{\Psi}_{lm}^{o\pm}}{dr}\right]. \tag{3.14}$$

Note this equation holds for both static and radiative modes.

We construct the inhomogeneous solutions to Eq. (3.2) via the standard variation of parameters method. As the source contains both a delta-function and the derivative of a delta-function the inhomogeneous solution and its radial derivative will both be discontinuous at the particle. Constructing the inhomogeneous solutions then becomes

a "matching" procedure with the jump in the field and its derivative across the particle governed by coefficients $\mathcal{S}_1$ and $\mathcal{S}_2$. Suppressing even/odd notation, we define matching coefficients as follows:

$$D^{\pm}_{lm} = \frac{1}{W_{lm}}\left[\left(\frac{\mathcal{S}_1}{f_0} + \frac{2M\mathcal{S}_2}{r_0^2 f_0^2}\right)\Psi^{\mp}_{lm} - \frac{\mathcal{S}_2}{f_0}\partial_r \Psi^{\mp}_{lm}\right], \quad (3.15)$$

with the usual Wronskian defined as $W_{lm} = f_0(\tilde{\Psi}^{-}_{lm}\partial_r\tilde{\Psi}^{+}_{lm} - \tilde{\Psi}^{+}_{lm}\partial_r\tilde{\Psi}^{-}_{lm})$. Finally we construct the inhomogeneous solutions via

$$\Psi^{\pm}_{lm}(r) = D^{\pm}_{lm}\tilde{\Psi}^{\pm}_{lm}(r). \quad (3.16)$$

where the $D^{\pm}_{lm}$'s are constants for all values of r.

To complete the metric perturbation in the RW gauge we use the $l = 0$ and $l = 1$ results of Zerilli [58]. Detweiler and Poisson expressed these contributions succinctly for circular orbits [59]. For the monopole and static dipole we have

$$h^{l=0}_{tt} = 2\mu\mathbb{E}_0\left(\frac{1}{r} + \frac{f}{r_0 - 2M}\right)\Theta(r - r_0), \quad (3.17)$$

$$h^{l=0}_{rr} = \frac{2\mu\mathbb{E}_0}{rf^2}\Theta(r - r_0), \quad (3.18)$$

$$h^{l=1,m=0}_{t\varphi} = -2\mu\mathbb{L}_0\sin^2\theta\begin{cases} r^2/r_0^3 & r < r_0 \\ 1/r & r > r_0 \end{cases}, \quad (3.19)$$

where Θ is the Heaviside step function and all other components are zero. The $l = 1$, $m = 1$ mode does not contribute to our gauge invariant quantities so we will not give the explicit expression for the nonzero h_{tt}, h_{tr} and h_{rr} components of this mode (but as a check we use the expressions, given as Eqs. (5.1)–(5.3) in Ref. [59], to check that the contribution from this mode to our invariants is identically zero).

As well as working in the RW gauge we also make a computation in the Lorenz gauge. Our code is a *Mathematica* reimplentation of that presented by Akcay [60] and as such we refer the reader to that work for further details.

A. Numerical computation of the retarded metric perturbation

For our RW gauge calculation, as discussed above, analytic solutions are known for the monopole, dipole and static ($m = 0$) modes. This only leaves the radiative modes ($l \geq 2$, $m \neq 0$) to be solved for numerically. Our numerical routines are implemented in *Mathematica* which allows us to go beyond machine precision in our calculation with ease. Given suitable boundary conditions near the black hole horizon and at a sufficiently large radius (we discuss below how we choose these radii in practice), we use *Mathematica*'s NDSolve routine to solve for the inner and outer solutions to the homogeneous Regge-Wheeler equation (3.2). Inhomogenous solutions are then constructed by imposing matching conditions of these functions at the location of the orbiting particle.

1. Numerical boundary conditions

In order to construct boundary conditions, we use an appropriate power law ansatz for Ψ_{RW} in the asymptotic regions close to spatial infinity and the horizon, given by

$$\tilde{\Psi}^{\infty}_{RW}(r) \sim e^{i\omega r_*}\sum_{n=0}^{n_+}\frac{a_n}{(\omega r)^n}, \quad (3.20)$$

$$\tilde{\Psi}^{\mathrm{H}}_{RW}(r) \sim e^{-i\omega r_*}\sum_{n=0}^{n_-} b_n f(r)^n. \quad (3.21)$$

Recursion relations for the series coefficients can be found by inserting our ansatz into the homogeneous RW equations, and choosing a maximum number of outer and inner terms $n_{\max} = n_{\pm}$ gives us initial values for our fields at these boundaries. Inserting (3.21) and (3.20) into (3.2) for the odd sector, we find the following recursion relations:

$$a_n = \frac{i}{2n}[(l(l+1) - n(n-1))a_{n-1} + 2M\omega(n-3)(n-1)a_{n-2}], \quad (3.22)$$

$$b_n = \frac{1}{n(n - 4iM\omega)}[(l(l+1) + 2n(n-1) - 3)a_{n-1} - (n+1)(n-3)a_{n-2}]. \quad (3.23)$$

As discussed above we do not need to solve the even sector field equations as we can transform from the simpler odd sector solutions using Eq. (3.14).

For the inner homogeneous solutions, the convergence of the series (3.21) improves with increasing n_-, and in practice we choose $n_- = 35$. The outer solutions require more care, as the boundary at infinity is an irregular singular point. Our expansion in Eq. (3.20) is an asymptotic series and, as such, the series is not strictly convergent in n for a fixed r. The ansatz will initially show power law convergence with increasing n, but for sufficiently high n the series will begin to diverge. At this point it is no longer

useful to add higher order terms. Note for a fixed max value n_+ the series will still converge with increasing r, as expected. After analysing this behavior, we take $n_+ = 100$ to get the best boundary conditions. Given the boundary expansions as a function of r, for fixed $n_\pm$, we must then choose a location for our boundary sufficiently close to $r_* = \pm\infty$ to give the desired accuracy. Setting the final term in our ansatz to be of order 10^{-d}, where d is our desired number of significant figures, we choose as our boundaries:

$$r_\infty = (a_{n_+} 10^d)^{1/n_+}, \tag{3.24}$$

$$r_H = 2M + (b_{n_-} 10^d)^{-1/n_-}. \tag{3.25}$$

The expansions (3.21) and (3.20) give the boundary conditions in terms of an arbitary overall amplitude, specified by a_0 and b_0. As we first construct homogeneous solutions we can set these amplitudes to any nonzero value, and in practice we choose $a_0 = b_0 = 1$. The amplitudes are then fixed by the matching procedure described above.

2. Numerical algorithm

In this section we briefly outline the steps we take in our numerical calculation in the Regge-Wheeler gauge. The Lorenz-gauge calculation follows a very similar set of steps [60].

(i) For each lm-mode with $l \geq 2$ solve the odd sector RW equation, even if $l + m =$ even. For the radiative modes ($l \geq 2$, $m \neq 0$) calculate boundary conditions for the homogeneous fields at $r_{H/\infty}$ using Eqs. (3.21) and (3.20). Using the boundary conditions, numerically integrate the homogeneous field equation (3.2) from the boundaries to the particle's orbit at $r = r_0$. For the static modes ($l \geq 2$, $m = 0$) evaluate the static homogeneous solutions (3.12)–(3.13) at the particle. Store the values of the inner and outer homogeneous fields and their radial derivatives at r_0.

(ii) For $l \geq 2$ and $l + m =$ even transform from the odd sector homogeneous solutions to the even sector homogeneous solutions using Eq. (3.14).

(iii) For all modes with $l \geq 2$ construct the inhomogeneous solutions via Eq. (3.16).

(iv) For the $l \geq 2$ modes reconstruct the metric perturbation using the formula in, e.g., Refs. [56].

(v) Complete the metric perturbation using the monopole and dipole solutions given in Eqs. (3.17)–(3.19).

(vi) Compute the retarded field l-mode (summed over m) contributions to the octupolar invariants using the formulas in Appendix A.

(vii) Construct the regularized l-modes using the tensor mode-sum approach described in Ref. [61]. The resulting contributions to the mode-sum accumulate rather slowly as l^{-2}.

(viii) Numerically fit for the unknown higher-order regularization parameters and use these to increase the rate of convergence of the mode-sum with l. This procedure is common in self-force calculations and is described in, e.g., Ref. [62].

(ix) To get the final result sum over l and make the shift to the asymptotically flat gauge as discussed in Appendix B.

For $r_0 \geq 4M$ we set the maximum computed l-mode to be $l_{\max} = 80$. This is sufficient to compute the octupolar invariants to high accuracy—see Sec. IV for details on the accuracy we obtain. For orbits with $3M < r_0 < 4M$ we find we need an increasing number of l-modes to achieve good accuracy in the final results, and for orbits near the light-ring (located at $r_0 = 3M$) we set $l_{\max} = 130$ in our code—see Sec. IV C.

B. Post-Newtonian expansion

The generation of analytic post-Newtonian expansions for the octupolar gauge invariants requires a calculation of the homogeneous solutions of the Regge-Wheeler equation for each ℓ mode. A general strategy for doing this was described in [63]. The calculation is broken into three sections: (i) the exact results of Zerilli give the $\ell = 0$, 1 components of the metric—see Eqs. (3.17)–(3.19), (ii) certain "low-ℓ" values calculated using the series solutions of Mano, Suzuki and Takasugi and (iii) "high-ℓ" contributions using a post-Newtonian ansatz. In a recent paper [43] this approach was optimized and improved allowing extremely high PN orders to be computed, which otherwise are only accessible by experimental mathematics techniques [41,42,64,65]. In the rest of this section we give a very brief overview of our technique and refer the reader to Ref. [43] for further details.

The analytic MST homogeneous solutions are expressed using an infinite series of hypergeometric functions denoted $X^{\rm in}_{\ell m}$, which satisfies the required boundary conditions at the horizon, and a series of irregular confluent hypergeometric functions, $X^{\rm up}_{\ell m}$, satisfying the boundary conditions as $r_* \to \infty$. Specifically we can write

$$X^{\rm in}_{\ell m} \sim B^{\rm trans}_{\ell m} e^{+i\omega r_*}, \qquad r_* \to -\infty$$
$$X^{\rm up}_{\ell m} \sim C^{\rm trans}_{\ell m} e^{-i\omega r_*}, \qquad r_* \to \infty$$

where $B^{\rm trans}_{\ell m}$ and $C^{\rm trans}_{\ell m}$ are the complex constants known as transmission coefficients, so that, with $a_0 = b_0 = 1$ in Eqs. (3.21) and (3.20), we have the identification

$$X^{\rm in}_{\ell m} = B^{\rm trans}_{\ell m} \tilde{\Psi}^{\rm H}_{RW} \tag{3.26}$$

$$X^{\rm up}_{\ell m} = C^{\rm trans}_{\ell m} \tilde{\Psi}^{\infty}_{RW}. \tag{3.27}$$

For the purposes of doing a PN expansion of the solutions for a particle on a circular orbit one finds two

natural and related small parameters, the frequency $\omega = m\Omega$ and the inverse of the radius, which is related to the orbital frequency Ω by $M\Omega = \sqrt{2GM/r^3}$. A natural way to deal with this double expansion is to instead expand in $\eta = 1/c$, and introduce two auxiliary variables $X_1 = GM/r$, $X_2{}^{1/2} = \omega r$, so that each instance of X_1 and X_2 must each come with an η^2 and are of the same order in the large-r limit. Expanding these solutions to a given PN order in this way amounts to truncating the $X^{\text{in/up}}$ infinite series at a finite order. However an in depth analysis of the series coefficients and the sometimes subtle behavior of the hypergeometric functions reveals a structure that can be exploited to optimize this truncation order and fine tune the length of the expansion of each term in the series.

A practical difficulty of this approach is that the MST series becomes increasingly large with higher η-order. For each PN order $y \sim \frac{1}{r_\Omega} \sim \eta^2$ so that to get say 10 PN, we need 20η powers. Significant further simplifications of these large series can be made rewriting the expansion as, for example,

$$X^{\text{in(MST)}}_{\ell m} = e^{i\psi^{\text{in}}} X_1{}^{-\ell-1-\sum_{j=1}^{\infty} a_{(6j,2j)}(2X_1X_2{}^{1/2}\eta^3)^{2j}} \times [1 + \eta^2 A_2^\ell + \eta^4 A_4^\ell + \eta^6 A_6^\ell + \cdots], \tag{3.28}$$

where the A_i are *strictly* polynomials in X_1, X_2. Since $2X_1X_2{}^{1/2} = 2GM\omega$, we see that ψ is r-independent allowing it to be essentially ignored as it will drop out with the Wronskian during normalization. We note that the purely even series in η includes some odd powers that appear at ℓ-dependent powers, and with these we also get extra unaccounted for log terms. For instance, for $\ell = 2$ the first odd term is at η^{13}.

As such, for a large-enough ℓ (dependent on the required expansion order), the homogeneous solutions become regular enough to instead use an ansatz of purely even powers as the solution of the RW equation. The details of this are described thoroughly in [43]. Once the homogeneous solutions of the Regge-Wheeler equation have been obtained, the even-parity solutions can be expressed using Eq. (3.14). This allows us to reconstruct the full metric perturbation, and from there our gauge invariant quantities, entirely from the Regge-Wheeler series solutions.

IV. RESULTS

In this section we present results for the octupolar invariants computed for circular orbits in a Schwarzschild background. More specifically, we present the six electric-type invariants defined in Eqs. (2.35a)–(2.35f), and the four magnetic-type invariants defined in Eqs. (2.38a)–(2.38d). In Sec. IV A we exhibit numerical data, and in Sec. IV B we supply post-Newtonian expansions. In Sec. IV C we examine the behavior of the invariants in the approach to the light-ring at $r = 3M$.

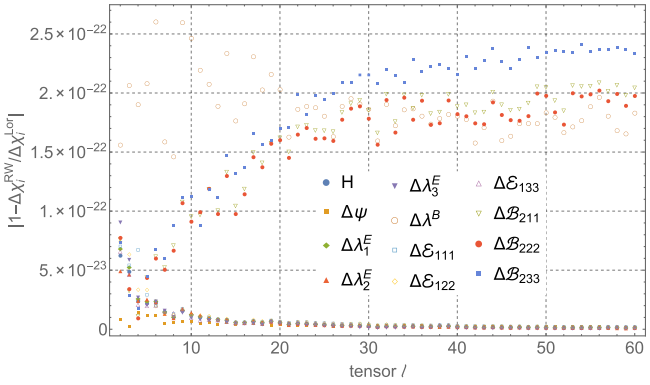

FIG. 1 (color online). Comparison of numerical results computed in the RW and Lorenz gauges for a variety of conservative gauge invariant quantities, $\Delta\chi_i$, along a circular orbit at $r_0 = 10M$. We see 22–24 significant digits agreement in the individual tensor l-modes of the retarded field.

A. Numerical data

We have employed two independent calculations in the Regge-Wheeler and Lorenz gauges: see Sec. III or Ref. [60] for details, respectively. Both codes are implemented in *Mathematica*, which allows us to go beyond machine precision. We find that the Regge-Wheeler and Lorenz gauge results for retarded field contribution to the invariants agree to around 22–24 significant figures. This high level of agreement, exemplified in Fig. 1, increases our confidence in the validity of the numerical calculation.

In Table I we present sample numerical results for the three conservative electric-type invariants. Table II provides the results for the three dissipative electric-type invariants. As the computation of the latter does not involve a regularization step, the dissipative results are considerably more accurate than for the conservative results. Our numerical results for the three conservative and one dissipative magnetic-type invariants are presented in Table III.

B. Post-Newtonian expansions

As outlined in Sec. III B, we have made a post-Newtonian calculation of the octupolar invariants using a method which builds upon the work of Ref. [43]. This method allows us to take the expansions to very high order. Results at 15th post-Newtonian order are available in an online repository [66]. Here, for brevity, we truncate the displayed results at a relatively low order:

TABLE I. Sample numerical results for the conservative electric-type octupolar invariants.

r_Ω/M	$\Delta\mathcal{E}_{111}$	$\Delta\mathcal{E}_{122}$	$\Delta\mathcal{E}_{133}$
4	-6.87640142×10^{-2}	5.634572704×10^{-2}	1.24182872×10^{-2}
5	$-1.3622429846\times10^{-2}$	$9.45418747546\times10^{-3}$	$4.1682423703\times10^{-3}$
6	$-5.61141083923\times10^{-3}$	$3.477232505498\times10^{-3}$	$2.13417833373\times10^{-3}$
7	$-2.925643118454\times10^{-3}$	$1.701979164325\times10^{-3}$	$1.223663954129\times10^{-3}$
8	$-1.710986615756\times10^{-3}$	$9.592475191788\times10^{-4}$	$7.517390965770\times10^{-4}$
9	$-1.075500995896\times10^{-3}$	$5.890480037652\times10^{-4}$	$4.864529921306\times10^{-4}$
10	$-7.120764484958\times10^{-4}$	$3.838876753995\times10^{-4}$	$3.281887730964\times10^{-4}$
12	$-3.494517915911\times10^{-4}$	$1.847169590917\times10^{-4}$	$1.647348324994\times10^{-4}$
14	$-1.913146810405\times10^{-4}$	$9.995537359206\times10^{-5}$	$9.135930744843\times10^{-5}$
16	$-1.133949991793\times10^{-4}$	$5.879346730837\times10^{-5}$	$5.460153187097\times10^{-5}$
18	$-7.141332604056\times10^{-5}$	$3.682750321689\times10^{-5}$	$3.458582282367\times10^{-5}$
20	$-4.718352028785\times10^{-5}$	$2.423514347706\times10^{-5}$	$2.294837681079\times10^{-5}$
30	$-9.514915883987\times10^{-6}$	$4.835793521499\times10^{-6}$	$4.679122362488\times10^{-6}$
40	$-3.040712519124\times10^{-6}$	$1.538289606495\times10^{-6}$	$1.502422912629\times10^{-6}$
50	$-1.252723439259\times10^{-6}$	$6.321181929625\times10^{-7}$	$6.206052462967\times10^{-7}$
60	$-6.064208487551\times10^{-7}$	$3.054930741569\times10^{-7}$	$3.009277745982\times10^{-7}$
70	$-3.282027079848\times10^{-7}$	$1.651475883984\times10^{-7}$	$1.630551195863\times10^{-7}$
80	$-1.927657419028\times10^{-7}$	$9.691577786310\times10^{-8}$	$9.584996403967\times10^{-8}$
90	$-1.205253640043\times10^{-7}$	$6.055682885677\times10^{-8}$	$5.996853514753\times10^{-8}$
100	$-7.917190975864\times10^{-8}$	$3.975890910078\times10^{-8}$	$3.941300065787\times10^{-8}$
500	$-1.277421047615\times10^{-10}$	$6.392477321681\times10^{-11}$	$6.381733154472\times10^{-11}$
1000	$-7.991970194046\times10^{-12}$	$3.997657790884\times10^{-12}$	$3.994312403162\times10^{-12}$
5000	$-1.279743808249\times10^{-14}$	$6.399252758926\times10^{-15}$	$6.398185323566\times10^{-15}$

TABLE II. Sample numerical results for the dissipative electric-type octupolar invariants.

r_Ω/M	$\Delta\mathcal{E}_{113}$	$\Delta\mathcal{E}_{223}$	$\Delta\mathcal{E}_{333}$
4	$1.43018712098924\times10^{-2}$	$-6.81363125080514\times10^{-3}$	$-7.48823995908726\times10^{-3}$
5	$1.69051912392376\times10^{-3}$	$-6.68228419170062\times10^{-4}$	$-1.02229070475370\times10^{-3}$
6	$3.93615041880796\times10^{-4}$	$-1.40326772303052\times10^{-4}$	$-2.53288269577744\times10^{-4}$
7	$1.24851076918558\times10^{-4}$	$-4.16707182592131\times10^{-5}$	$-8.31803586593453\times10^{-5}$
8	$4.78575862364605\times10^{-5}$	$-1.52593581419753\times10^{-5}$	$-3.25982280944852\times10^{-5}$
9	$2.09252624095044\times10^{-5}$	$-6.45207930480653\times10^{-6}$	$-1.44731831046978\times10^{-5}$
10	$1.00921765694192\times10^{-5}$	$-3.03317966765418\times10^{-6}$	$-7.05899690176504\times10^{-6}$
12	$2.90853534249746\times10^{-6}$	$-8.42878520552755\times10^{-7}$	$-2.06565682194470\times10^{-6}$
14	$1.02905687355232\times10^{-6}$	$-2.90962875240999\times10^{-7}$	$-7.38093998311317\times10^{-7}$
16	$4.21307269886127\times10^{-7}$	$-1.17032511794287\times10^{-7}$	$-3.04274758091840\times10^{-7}$
18	$1.92451417988312\times10^{-7}$	$-5.27522804430828\times10^{-8}$	$-1.39699137545229\times10^{-7}$
20	$9.57423553217574\times10^{-8}$	$-2.59726822309717\times10^{-8}$	$-6.97696730907857\times10^{-8}$
30	$6.63075048503344\times10^{-9}$	$-1.74627612621227\times10^{-9}$	$-4.88447435882117\times10^{-9}$
40	$1.00806706036123\times10^{-9}$	$-2.61810134057605\times10^{-10}$	$-7.46256926303620\times10^{-10}$
50	$2.34720446527898\times10^{-10}$	$-6.04700459200130\times10^{-11}$	$-1.74250400607885\times10^{-10}$
60	$7.14698583248068\times10^{-11}$	$-1.83158348544703\times10^{-11}$	$-5.31540234703365\times10^{-11}$
70	$2.61736513652863\times10^{-11}$	$-6.68285229858544\times10^{-12}$	$-1.94907990667008\times10^{-11}$
80	$1.09692221205352\times10^{-11}$	$-2.79307929655166\times10^{-12}$	$-8.17614282398351\times10^{-12}$
90	$5.09523969822615\times10^{-12}$	$-1.29465822904663\times10^{-12}$	$-3.80058146917952\times10^{-12}$
100	$2.56663032262918\times10^{-12}$	$-6.51067248226772\times10^{-13}$	$-1.91556307440241\times10^{-12}$
500	$7.32252735609857\times10^{-17}$	$-1.83582572460285\times10^{-17}$	$-5.48670163149571\times10^{-17}$
1000	$8.09167955607435\times10^{-19}$	$-2.02577720909791\times10^{-19}$	$-6.06590234697644\times10^{-19}$
5000	$2.31673725041822\times10^{-23}$	$-5.79347353907946\times10^{-24}$	$-1.73738989651028\times10^{-23}$

TABLE III. Sample numerical results for the magnetic-type octupolar invariants.

r_Ω/M	$\Delta\mathcal{B}_{211}$	$\Delta\mathcal{B}_{222}$	$\Delta\mathcal{B}_{233}$	$\Delta\mathcal{B}_{123}$
4	$-6.148298254370\times10^{-2}$	$5.070286329453\times10^{-2}$	$1.078011924917\times10^{-2}$	$1.07801192491724\times10^{-2}$
5	$-9.558323357929\times10^{-3}$	$7.670992694990\times10^{-3}$	$1.887330662938\times10^{-3}$	$1.88733066293848\times10^{-3}$
6	$-3.155936380263\times10^{-3}$	$2.476758241817\times10^{-3}$	$6.791781384454\times10^{-4}$	$6.79178138445361\times10^{-4}$
7	$-1.397948966284\times10^{-3}$	$1.081923065789\times10^{-3}$	$3.160259004949\times10^{-4}$	$3.16025900494923\times10^{-4}$
8	$-7.234703923371\times10^{-4}$	$5.550936330078\times10^{-4}$	$1.683767593293\times10^{-4}$	$1.68376759329306\times10^{-4}$
9	$-4.130973443372\times10^{-4}$	$3.151840931693\times10^{-4}$	$9.791325116795\times10^{-5}$	$9.79132511679517\times10^{-5}$
10	$-2.528015715619\times10^{-4}$	$1.921517184307\times10^{-4}$	$6.064985313116\times10^{-5}$	$6.06498531311616\times10^{-5}$
12	$-1.095551773983\times10^{-4}$	$8.288773695651\times10^{-5}$	$2.666744044177\times10^{-5}$	$2.66674404417714\times10^{-5}$
14	$-5.444485917231\times10^{-5}$	$4.108569884562\times10^{-5}$	$1.335916032669\times10^{-5}$	$1.33591603266878\times10^{-5}$
16	$-2.980264003325\times10^{-5}$	$2.245424872606\times10^{-5}$	$7.348391307187\times10^{-6}$	$7.34839130718667\times10^{-6}$
18	$-1.753993694654\times10^{-5}$	$1.320134773357\times10^{-5}$	$4.338589212967\times10^{-6}$	$4.33858921296681\times10^{-6}$
20	$-1.092394842331\times10^{-5}$	$8.215915676267\times10^{-6}$	$2.708032747040\times10^{-6}$	$2.70803274704046\times10^{-6}$
30	$-1.770249199828\times10^{-6}$	$1.329249843091\times10^{-6}$	$4.409993567363\times10^{-7}$	$4.40999356736253\times10^{-7}$
40	$-4.868817160862\times10^{-7}$	$3.653967138885\times10^{-7}$	$1.214850021976\times10^{-7}$	$1.21485002197624\times10^{-7}$
50	$-1.788310960062\times10^{-7}$	$1.341778109443\times10^{-7}$	$4.465328506186\times10^{-8}$	$4.46532850618555\times10^{-8}$
60	$-7.887212354333\times10^{-8}$	$5.917061308384\times10^{-8}$	$1.970151045949\times10^{-8}$	$1.97015104594935\times10^{-8}$
70	$-3.946891664217\times10^{-8}$	$2.960771807198\times10^{-8}$	$9.861198570192\times10^{-9}$	$9.86119857019213\times10^{-9}$
80	$-2.166444813367\times10^{-8}$	$1.625085708368\times10^{-8}$	$5.413591049991\times10^{-9}$	$5.41359104999132\times10^{-9}$
90	$-1.276212037585\times10^{-8}$	$9.572758888543\times10^{-9}$	$3.189361487310\times10^{-9}$	$3.18936148731046\times10^{-9}$
100	$-7.948907544564\times10^{-9}$	$5.962268324527\times10^{-9}$	$1.986639220037\times10^{-9}$	$1.98663922003664\times10^{-9}$
500	$-5.716760192009\times10^{-12}$	$4.287586670256\times10^{-12}$	$1.429173521752\times10^{-12}$	$1.42917352175245\times10^{-12}$
1000	$-2.528141980419\times10^{-13}$	$1.896108307399\times10^{-13}$	$6.320336730204\times10^{-14}$	$6.32033673020413\times10^{-14}$
5000	$-1.809952182177\times10^{-16}$	$1.357464188697\times10^{-16}$	$4.524879934796\times10^{-17}$	$4.52487993479633\times10^{-17}$

$$\Delta\mathcal{E}_{111} = -8y^4 + 8y^5 + 30y^6 - \left(\frac{1711}{6} - \frac{4681}{512}\pi^2\right)y^7 + \left(\frac{136099}{400} - \frac{6255}{1024}\pi^2 - \frac{2048}{5}\gamma - \frac{4096}{5}\log 2 - \frac{1024}{5}\log y\right)y^8 - \left(\frac{1604627}{630} - \frac{6413231}{49152}\pi^2 - \frac{159664}{105}\gamma - \frac{18416}{5}\log 2 + \frac{4374}{7}\log 3 - \frac{79832}{105}\log y\right)y^9 - \frac{219136}{525}\pi y^{19/2} + \mathcal{O}(y^{10}), \tag{4.1}$$

$$\Delta\mathcal{E}_{122} = 4y^4 - \frac{7}{3}y^5 - 9y^6 + \left(\frac{1369}{8} - \frac{9677}{2048}\pi^2\right)y^7 + \left(\frac{121369}{7200} + \frac{265}{192}\pi^2 + \frac{1024}{5}\gamma + \frac{2048}{5}\log 2 + \frac{512}{5}\log y\right)y^8 - \left(\frac{132611239}{120960} - \frac{240298535}{1179648}\pi^2 + \frac{173416}{315}\gamma + \frac{53416}{35}\log 2 - \frac{2916}{7}\log 3 + \frac{86708}{315}\log y\right)y^9 + \frac{109568}{525}\pi y^{19/2} + \mathcal{O}(y^{10}), \tag{4.2}$$

$$\Delta\mathcal{E}_{133} = 4y^4 - \frac{17}{3}y^5 - 21y^6 + \left(\frac{2737}{24} - \frac{9047}{2048}\pi^2\right)y^7 - \left(\frac{2571151}{7200} - \frac{14525}{3072}\pi^2 - \frac{1024}{5}\gamma - \frac{2048}{5}\log 2 - \frac{512}{5}\log y\right)y^8 + \left(\frac{62957089}{17280} - \frac{394216079}{1179648}\pi^2 - \frac{305576}{315}\gamma - \frac{75496}{35}\log 2 + \frac{1458}{7}\log 3 - \frac{152788}{315}\log y\right)y^9 + \frac{109568}{525}\pi y^{19/2} + \mathcal{O}(y^{10}), \tag{4.3}$$

$$\Delta\mathcal{E}_{113} = \frac{128}{5}y^{13/2} - \frac{108}{5}y^{15/2} + \frac{512}{5}\pi y^8 - \frac{46978}{105}y^{17/2} + \frac{3794}{45}\pi y^9 + \frac{8}{496125}(107554351 + 8467200\pi^2 - 25885440\gamma - 51770880\log 2 - 12942720\log y)y^{19/2} + \mathcal{O}(y^{10}), \tag{4.4}$$

$$\Delta\mathcal{E}_{223} = -\frac{32}{5}y^{13/2} - \frac{18}{5}y^{15/2} - \frac{128}{5}\pi y^8 + \frac{8276}{105}y^{17/2} - \frac{15242}{315}\pi y^9 - \frac{1}{496125}(152535527 + 16934400\pi^2 - 51770880\gamma - 103541760\log 2 - 25885440\log y)y^{19/2} + \mathcal{O}(y^{10}), \tag{4.5}$$

$$\Delta\mathcal{E}_{333} = -\frac{96}{5}y^{13/2} + \frac{126}{5}y^{15/2} - \frac{384}{5}\pi y^8 + \frac{38702}{105}y^{17/2} - \frac{3772}{105}\pi y^9 - \frac{1}{165375}(235966427 + 16934400\pi^2 - 51770880\gamma - 103541760\log 2 - 25885440\log y)y^{19/2} + \mathcal{O}(y^{10}), \tag{4.6}$$

$$\Delta\mathcal{B}_{123} = \frac{64}{3}y^7 + \frac{36}{5}y^8 + \frac{256}{3}\pi y^{17/2} - \frac{5347}{15}y^9 + \frac{2197}{15}\pi y^{19/2} + \frac{4}{11025}(3475113 + 313600\pi^2 - 958720\gamma - 1917440\log 2 - 479360\log y)y^{10} - \frac{10961}{7}\pi y^{21/2} + \mathcal{O}(y^{11}), \tag{4.7}$$

$$\begin{aligned}\Delta\mathcal{B}_{211} = {} & -8y^{9/2} + \frac{16}{3}y^{11/2} - 20y^{13/2} + \left(-\frac{677}{2} + \frac{5101}{512}\pi^2\right)y^{15/2} \\ & - \frac{1}{230400}(246270016 - 20642025\pi^2 + 94371840\gamma + 188743680\log 2 + 47185920\log y)y^{17/2} \\ & - \frac{1}{154828800}(417740314624 - 17848070625\pi^2 - 131939696640\gamma - 390644367360\log 2 \\ & + 123619737600\log 3 - 65969848320\log y)y^{19/2} - \frac{219136}{525}\pi y^{10} + \mathcal{O}(y^{21/2}),\end{aligned} \tag{4.8}$$

$$\begin{aligned}\Delta\mathcal{B}_{222} = {} & 6y^{9/2} - 4y^{11/2} + \frac{83}{4}y^{13/2} + \left(\frac{1069}{4} - \frac{7809}{1024}\pi^2\right)y^{15/2} \\ & + \frac{1}{204800}(234195584 - 19194125\pi^2 + 62914560\gamma + 125829120\log 2 + 31457280\log y)y^{17/2} \\ & + \frac{1}{11468800}(125170823168 - 11193257425\pi^2 - 5923143680\gamma - 19177144320\log 2 \\ & + 7166361600\log 3 - 2961571840\log y)y^{19/2} + \frac{54784}{175}\pi y^{10} + \mathcal{O}(y^{21/2}),\end{aligned} \tag{4.9}$$

$$\begin{aligned}\Delta\mathcal{B}_{233} = {} & 2y^{9/2} - \frac{4}{3}y^{11/2} - \frac{3}{4}y^{13/2} + \left(\frac{285}{4} - \frac{2393}{1024}\pi^2\right)y^{15/2} \\ & - \frac{1}{1843200}(137600128 - 7610925\pi^2 - 188743680\gamma - 377487360\log 2 - 94371840\log y)y^{17/2} \\ & - \frac{1}{309657600}(2544131596288 - 266521809225\pi^2 + 103954513920\gamma + 263505838080\log 2 \\ & - 53747712000\log 3 + 51977256960\log y)y^{19/2} + \frac{54784}{525}\pi y^{10} + \mathcal{O}(y^{21/2}),\end{aligned} \tag{4.10}$$

where here $y = M/r_0$.

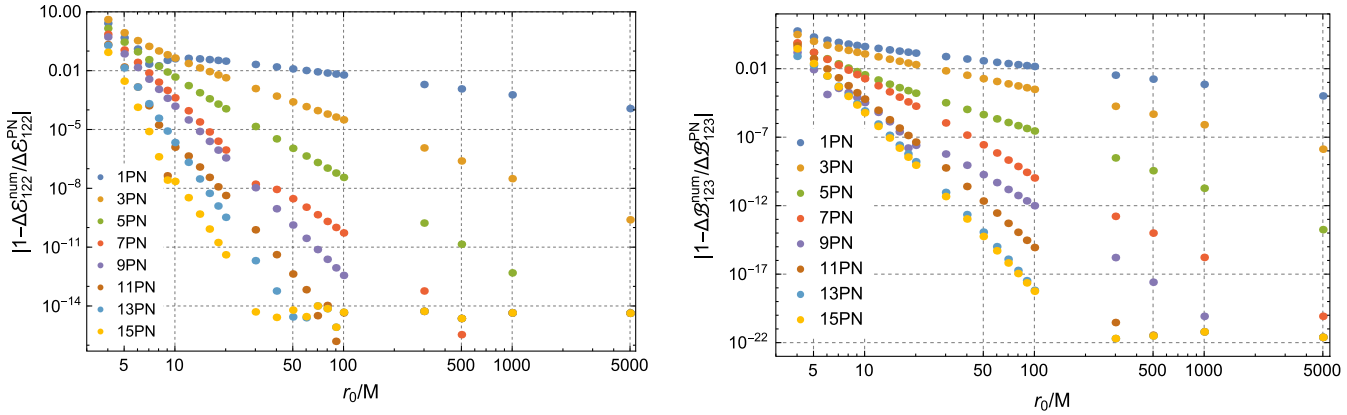

FIG. 2 (color online). Comparison of our numerical and PN results for (left) $\Delta\mathcal{E}_{122}$ and (right) $\Delta\mathcal{B}_{123}$. For each invariant we plot the relative difference between the numerical data and successive truncations of the relevant PN series, i.e., in the legend "xPN" means we are comparing against the PN series with all terms up to and including (relative) xPN order. As successive PN terms are added the agreement between the PN series and the numerical results improves. For the conservative invariants, such as $\Delta\mathcal{E}_{122}$, the agreement between the PN series and the numerical data saturates at a relative accuracy of 13–14 significant figures. For the dissipative invariants, such as $\Delta\mathcal{B}_{123}$, the comparison saturates at 21–22 significant figures. This difference in accuracy in the numerical data stems from the requirement to regularize the conservative invariants whereas the dissipative invariants do not require regularization.

Figure 2 shows sample comparisons of our PN and numerical results. We observe that, as higher-order PN terms are included in the comparison, the agreement improves for all values of r_0. For large orbital radii the comparison saturates at the level of our (smaller than machine precision) numerical round-off error. For strong-field orbits, the comparison allows us to estimate how well the PN series performs in this regime. At $r_0 = 10M$ we typically find that the 15PN series recovers the first 7–8 significant digits of the numerical result. At the innermost stable circular orbit, at $r_0 = 6M$, the 15PN series successfully recovers the first 3–4 significant figures. The excellent agreement we observe between our PN and numerical calculations gives us further confidence in both sets of results.

C. Behavior near the light-ring

With our numerical codes we can calculate the behavior of the octupolar invariants as the orbit approaches the light-ring at $r_0 = 3M$. In general, the invariants will diverge as the light-ring is approached, and knowledge of the rate of divergence, along with our high-order PN results and our other numerical results, may be useful in performing global fits for the invariants across all orbital radii. Such fits find utility in EOB theory and already results for the redshift, spin precession and tidal invariants have been employed in EOB models [25–27]. In this section we discuss, and give results for, the rate of divergence of the invariants near the light-ring but stop short of making global fits for the invariants.

The main challenge in computing conservative invariants near the light-ring is the late onset of convergence of the mode-sum in this regime (see Ref. [25] for a discussion of this behavior). This necessitates computing a great deal more lm-modes; typically we set $l_{\max} = 130$ for our calculations in this regime. By comparison, for orbits with $r_0 = 4M$ we use $l_{\max} = 80$. Not only then do we need to numerically compute an additional 8085 lm-modes, on top of the 3239 modes required to reach $l_{\max} = 80$, but these higher lm-modes are more challenging to calculate

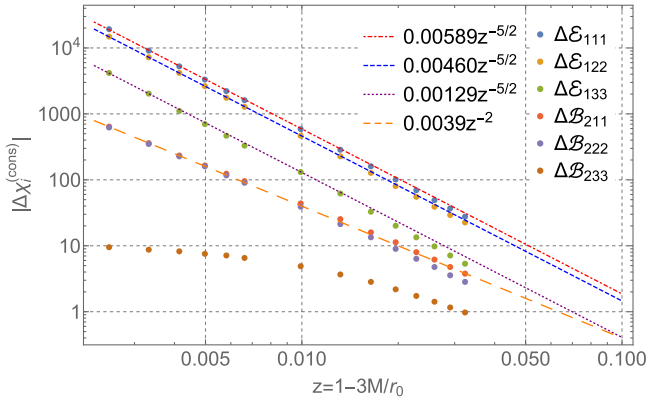

FIG. 3 (color online). Divergence of the conservative octupolar invariants as the orbital radius approaches the light-ring. The electric-type invariants, $\Delta\mathcal{E}_{111}$, $\Delta\mathcal{E}_{122}$, $\Delta\mathcal{E}_{133}$, diverge as $z^{-5/2}$ where $z = 1 - 3M/r_0$. Two of the magnetic-type invariants, $\Delta\mathcal{B}_{211}$ and $\Delta\mathcal{B}_{222}$, are observed to diverge as z^{-2}. We are unable to accurately deduce the rate of the divergence $\Delta\mathcal{B}_{233}$ but we plot our numerical results to show that its rate of divergence is subdominant to the other invariants.

numerically owing to the stronger power-law growth near the particle for high l and the high mode frequency (and thus large number of oscillations that need to be resolved far from the particle) for high m-modes. These considerations mean that numerical calculations at radii near the light-ring are substantially more computationally expensive than our other numerical results.

Our main results are presented in Fig. 3. We are able to infer the rate of divergence of five out of six of the electric- and magnetic-type invariants. Defining $z \equiv 1-3M/r_0$ we find $\Delta\mathcal{E}_{111} \sim -0.00589 z^{-5/2}$, $\Delta\mathcal{E}_{122} \sim 0.00406 z^{-5/2}$, $\Delta\mathcal{E}_{133} \sim 0.0129 z^{-5/2}$, $\mathcal{B}_{211} \sim -0.0039 z^{-2}$ and $\mathcal{B}_{222} \sim 0.0039 z^{-2}$ as $z \to 0$. For the remaining conservative invariant, $\Delta\mathcal{B}_{233}$, our current results are not sufficient to accurately determine the divergence rate, but we can say that the rate is subdominant to the other invariants.

V. APPLICATIONS

Here we briefly outline two possible applications of the results of Sec. IV: in informing EOB theory, and in refining initial data for binary black hole simulations with large mass ratios in the strong field.

A. Informing EOB theory

In EOB theory, the dynamics of binary systems are reformulated in terms of the dynamics of a single "effective" body moving in a metric $ds^2 = -A(u;\nu)dt^2 + B(u;\nu)d\hat{r}^2 + \hat{r}^2(d\theta^2 + \sin^2\theta d\phi^2)$ (nonspinning case), where $A(u;\nu)$ and $B(u;\nu)$ are smooth functions of inverse radius $u = (M+\mu)/\hat{r}$ and symmetric mass ratio $\nu = \mu M/(\mu+M)^2$. For tidal interactions, it was proposed in Ref. [67] that the metric function should take the form $A = A^{\rm BBH} + A_1^{\rm tidal} + A_2^{\rm tidal}$. The latter terms are radial potentials associated with tidal deformations of bodies 1 and 2, which may be decomposed into multipolar contributions, $A_1^{\rm tidal} = A_1^{(2+)} + A_1^{(2-)} + A_1^{(3+)} + A_1^{(3-)} \ldots$, from the electric quadrupole ($A_1^{(2+)}$), magnetic quadrupole ($A_1^{(2-)}$), electric octupole ($A_1^{(3+)}$), magnetic octupole ($A_1^{(3-)}$) sectors, respectively, etc. In Ref. [67] a relationship was established between the *dynamically*-significant tidal functions $A_i^{(j\pm)}$ and *kinematically*-invariant functions $J_\bullet(y)$ formed from the tidal tensors (see Eq. (6.11) in Ref. [27]). In the quadrupolar sector, the relevant invariants are

$$J_{e^2} \equiv \mathcal{E}_{ab}\mathcal{E}^{ab}, \qquad J_{b^2} \equiv \mathcal{B}_{ab}\mathcal{B}^{ab}, \qquad J_{e^3} \equiv \mathcal{E}_{ab}\mathcal{E}^{bc}\mathcal{E}^{a}_{c}, \ldots \tag{5.1}$$

TABLE IV. Sample numerical results for the $\hat{\delta}_{K3+}$ as defined in Eq. (2.47).

r_Ω/M	$\hat{\delta}_{K3+}$
4	−1.072402291940
5	−0.952268599881
6	−1.150905925689
7	−1.347913915585
8	−1.511472597166
9	−1.643850731891
10	−1.751437199028
12	−1.913557269058
14	−2.028682058336
16	−2.114109122984
18	−2.179795496907
20	−2.231771587180
30	−2.383995972376
40	−2.457665106706
50	−2.500976521370
60	−2.529455493583
70	−2.549596340465
80	−2.564588968234
90	−2.576181641423
100	−2.585412146067
500	−2.650685806947
1000	−2.658693616512
5000	−2.665074853918

In the electric-octupolar sector, the relevant quantities are (see Appendix D of [27]) $J_{3+} = K_{3+} + \frac{1}{3}J_{\dot{2}+}$, where $K_{3+} \equiv \mathcal{E}_{abc}\mathcal{E}^{abc}$ and $J_{\dot{2}+} \equiv \mathcal{E}_{ab0}\mathcal{E}^{ab0}$. In the magnetic-octupolar sector, analogous quantities may be formed.

The $\mathcal{O}(\mu)$ part of these invariants may be easily deduced from our octupolar components $\Delta\mathcal{E}_{111}, \ldots$. For example, ΔK_{3+}, obtained via Eq. (2.15), is related to $\hat{\delta}_{K3+}$ by (2.47).

Previously, Bini and Damour have given a PN expansion of $\hat{\delta}_{K3+}$ to 7.5PN order (see Eq. (D10) in Ref. [27]). With the results of Sec. IV, we are able to go a step further. First, in Table IV we give numerical data for $\hat{\delta}_{K3+}$ in the strong-field regime. The data indicates that $\hat{\delta}_{K3+}$ has a local maximum somewhat within the innermost stable circular orbit. Second, in an online repository [66], we provide a higher-order PN expansion of $\hat{\delta}_{K3+}$; below, we state the expansion at 8.5PN order (correcting a minor transcription error in the y^6 term of (D10) in Ref. [27]):

$$\hat{\delta}_{K3+} = -\frac{8}{3}+\frac{358}{45}y+\frac{11848}{675}y^2+\left(-\frac{3581903}{40500}+\frac{4681}{1536}\pi^2\right)y^3$$
$$+\left(\frac{614794483}{2430000}-\frac{790931}{92160}\pi^2-\frac{2048}{15}\gamma-\frac{4096}{15}\log 2-\frac{1024}{15}\log y\right)y^4$$
$$+\left(-\frac{759123028241}{1020600000}+\frac{431520437}{11059200}\pi^2+\frac{1070704}{1575}\gamma+\frac{354064}{225}\log 2-\frac{1458}{7}\log 3+\frac{535352}{1575}\log y\right)y^5$$
$$-\frac{219136}{1575}\pi y^{11/2}+\left(\frac{12569905047667}{2187000000}-\frac{1903269674027}{1769472000}\pi^2-\frac{42147341}{6291456}\pi^4+\frac{181080056}{212625}\gamma-\frac{123628168}{212625}\log 2\right.$$
$$\left.+\frac{73953}{35}\log 3+\frac{90540028}{212625}\log y\right)y^6+\frac{118163398}{165375}\pi y^{13/2}+y^7\left(\frac{52369829422440012073}{990186120000000}-\frac{4176344893416403}{990904320000}\pi^2\right.$$
$$+\frac{351206984461}{6039797760}\pi^4-\frac{4143716714678}{245581875}\gamma+\frac{1753088}{1575}\gamma^2-\frac{6124042466966}{245581875}\log 2+\frac{7012352}{1575}\gamma\log 2$$
$$+\frac{7012352}{1575}\log^2 2-\frac{214350489}{30800}\log 3+\frac{9765625}{14256}\log 5-\frac{2071858357339}{245581875}\log y+\frac{1753088}{1575}\gamma\log y$$
$$\left.+\frac{3506176}{1575}\log 2\log y+\frac{438272}{1575}\log^2 y-\frac{32768}{15}\zeta(3)\right)+\frac{169822838237}{245581875}\pi y^{15/2}$$
$$+y^8\left(\frac{12344050867662917568550 79}{10812832430400000000}-\frac{20516582870304319}{9754214400000}\pi^2-\frac{4004468043930067}{11596411699200}\pi^4\right.$$
$$+\frac{6403209826927357}{335219259375}\gamma-\frac{819289024}{165375}\gamma^2+\frac{18668500151420029}{335219259375}\log 2-\frac{4048635776}{165375}\gamma\log 2-\frac{4434375616}{165375}\log^2 2$$
$$-\frac{4137804755289}{196196000}\log 3+\frac{227448}{49}\gamma\log 3+\frac{227448}{49}\log 2\log 3+\frac{113724}{49}\log^2 3-\frac{8837890625}{1111968}\log 5$$
$$+\frac{6300230470447357}{670438518750}\log y-\frac{819289024}{165375}\gamma\log y-\frac{2024317888}{165375}\log 2\log y+\frac{113724}{49}\log 3\log y$$
$$\left.-\frac{204822256}{165375}\log^2 y+\frac{10678144}{1575}\zeta(3)\right)+\left(-\frac{1048639996225198903}{58998589650000}\pi-\frac{3506176}{4725}\pi^3+\frac{375160832}{165375}\pi\gamma\right.$$
$$\left.+\frac{750321664}{165375}\pi\log 2+\frac{187580416}{165375}\pi\log y\right)y^{17/2}+\mathcal{O}(y^9). \tag{5.2}$$

B. Informing initial data models

How does a black hole move through and respond to an external environment? This question has been addressed by Manasse [68], and others [45–47,69–75], via the method of matched asymptotic expansions (MAE). In scenarios with two distinct length scales (m_1, $m_2 \ll r_{12}$ where r_{12} is the orbital separation), one may attempt to match "inner" and "outer" expansions across a suitable "buffer" zone (m_1, $m_2 \ll r \ll r_{12}$) [76]. Indeed, this method was applied to derive the equations of motion underpinning the self-force approach [28]. Recently, much work has gone into improving initial data for simulations of binary black hole inspirals using MAEs [45,48,49,77–80].

In a standard approach [47,69,72,73], the black hole is tidally distorted by "external multipole moments": spatial, symmetric, tracefree (STF) tensors $\mathbb{E}_{ij}$, $\mathbb{B}_{ij}$, $\mathbb{E}_{ijk}$, $\mathbb{B}_{ijk}$, etc., related to the Riemann tensor evaluated on the worldline in the *regular* perturbed spacetime. These STF tensors are essentially equivalent to our tetrad-resolved quantities; for example, Detweiler's [72] STF moments are given by $\mathbb{E}_{ij} = \mathcal{E}_{ij}$, $\mathbb{B}_{ij} = \mathcal{B}_{ij}$, $\mathbb{E}_{ijk} = \mathcal{E}_{ijk}$ and $\mathbb{B}_{ijk} = \frac{3}{4}\mathcal{B}_{ijk}$, with the subtlety of the interchange of spatial indices $2 \leftrightarrow 3$.

Johnson-McDaniel *et al.* [45] have applied the MAE method to "stitch" two tidally-perturbed Schwarzschild black holes into an external PN metric. Implicit in Eqs. (B1a)–(B1d) of Ref. [45] is a PN expansion of (conservative) quadrupolar and octupolar tidal quantities. Restricting to $\mathcal{O}(\mu)$, in our notation Eqs. (B1a)–(B1d) of [45] imply

$$M^3\mathcal{E}_{111} = 6y^4+3y^5+\frac{\mu}{M}(-8y^4+8y^5)+\mathcal{O}(y^6,\mu^2) \tag{5.3}$$

$$M^3\mathcal{E}_{122} = -3y^4 - 4y^5 + \frac{\mu}{M}\left(4y^4 - \frac{7}{3}y^5\right) + \mathcal{O}(y^6, \mu^2) \tag{5.4}$$

$$M^3\mathcal{E}_{133} = -3y^4 + y^5 + \frac{\mu}{M}\left(4y^4 - \frac{17}{3}y^5\right) + \mathcal{O}(y^6, \mu^2) \tag{5.5}$$

$$M^3\mathcal{B}_{211} = 8y^{9/2} + \frac{\mu}{M}(-8y^{9/2}) + \mathcal{O}(y^{11/2}, \mu^2) \tag{5.6}$$

$$M^3\mathcal{B}_{222} = -6y^{9/2} + \frac{\mu}{M}(6y^{9/2}) + \mathcal{O}(y^{11/2}, \mu^2) \tag{5.7}$$

$$M^3\mathcal{B}_{233} = -2y^{9/2} + \frac{\mu}{M}(2y^{9/2}) + \mathcal{O}(y^{11/2}, \mu^2). \tag{5.8}$$

Note that here the $\mathcal{O}(\mu^0)$ terms are leading-order terms in the Taylor expansion of the "background" Schwarzschild results, and the $\mathcal{O}(\mu^1)$ terms are consistent with the leading terms of our PN series in Sec. IV B. This reassuring consistency suggests that our $\mathcal{O}(\mu/M)$ results may indeed be used to help improve initial data for large mass-ratio binaries in the latter stages of inspiral.

VI. DISCUSSION AND CONCLUSION

In the preceding sections we have pursued the line of enquiry of Refs. [27,31,35,37], concerned with identifying and calculating $\mathcal{O}(\mu)$ invariants for circular orbits, onwards into the octupolar sector. We identified 7 independent degrees of freedom in the octupolar sector, given by the (symmetrized) components of the derivative of the Riemann tensor as decomposed in the electric-quadrupole basis. A complete set of octupolar invariants for circular orbits is given by, e.g., $\Delta\mathcal{E}_{111}$, $\Delta\mathcal{E}_{122}$, $\Delta\mathcal{B}_{211}$, $\Delta\mathcal{B}_{222}$, $\Delta\mathcal{E}_{311}$, $\Delta\mathcal{E}_{322}$, $\Delta\mathcal{B}_{123}$. Here, the first four are conservative and the latter three are dissipative in character. The remaining symmetrized components $\Delta\mathcal{E}_{133}$, $\Delta\mathcal{B}_{233}$ (conservative) and $\Delta\mathcal{E}_{333}$ (dissipative) follow from trace conditions. All additional octupolar components, ΔE_{ij0}, ΔB_{ij0}, $\Delta E_{i[jk]}$ and $\Delta B_{i[jk]}$, may be written in terms of the previous-known quadrupolar tidal invariants $\Delta\mathcal{E}_{11}$, $\Delta\mathcal{E}_{22}$, $\Delta\mathcal{B}_{12}$, $\Delta\mathcal{B}_{23}$ [37], the spin-precession invariant $\Delta\psi$ [35] and the redshift invariant ΔU [31]. Accurate results for the latter quantities are provided in Tables I and III of Ref. [37] and PN series are given in Ref. [43]. In passing, we should note a relationship which was overlooked in Ref. [37]: $\Delta\mathcal{B}_{23} = -\tilde{\mathcal{B}}_{12}\Delta\chi$, where $\Delta\chi$ is the dissipative invariant of Table I in Ref. [37]. Also, we should recall that the temporal and azimuthal components of the self-force define one more dissipative invariant, $F_t = \Omega F_\phi$. Taken together, we believe we have now arrived at a complete characterization of all circular-orbit invariants in the regular perturbed spacetime through $\mathcal{O}(\mu)$, up to third-derivative order.

Highly accurate numerical results for all the octupolar invariants are given in Tables I–IV. Our numerical calculation is performed using *Mathematica* and is made within the Regge-Wheeler gauge as described in Sec. III. In addition, as a cross-check on our results, we performed the same calculation in the Lorenz gauge using a *Mathematica* re-implementation of Ref. [60]—see Fig. 1 for an example of the excellent agreement we find between the two calculations. To complement our numerical results, we also calculate high-order post-Newtonian expansions for all the invariants. Our technique is briefly described in Sec. III B with the full details given in Ref. [43]. The lower-order PN expansions are given in Sec. IV B with the higher-order terms available online [66]. In Sec. V we explored two possible applications for the octupolar invariants.

We can envisage several ways this work could be extended. First, the high-order post-Newtonian results and the strong-field numerical data could be combined to produce *global* semianalytic fits for the various invariants. Here, knowledge of the behavior at the light-ring (Sec. IV C) should prove useful. Similar fits for other invariants have already been applied to EOB models [25,26,38] and freshly-calibrated EOB models have been successfully compared against numerical relativity simulations [6]. Second, we note that in Sec. II we have, in fact, derived the form of the octupolar invariants for circular, equatorial orbits in a *rotating* black hole spacetime. Looking ahead, practical calculations on Kerr spacetime are needed. The redshift invariant has already been calculated for circular, equatorial orbits about a Kerr black hole [40,53]. It seems a natural extension to extend other invariants, such as the ones we describe here, to the rotating scenario. We believe this should be pursued with both numerical and high-order post-Newtonian treatments. Third, a further natural extension is to consider invariants for noncircular orbits. This was recently explored by Akcay *et al.* [39] for the redshift invariant and we expect the calculation for other invariants to follow in time. Fourth, looking further into the future, invariants at second order in the mass ratio could be calculated. The necessary regularization procedure is now known [81–83] and the framework for making practical calculations is beginning to emerge [84,85]. As with previous calculations, initial work will focus on the redshift invariant [86] but the calculation of other invariants will surely follow.

ACKNOWLEDGMENTS

We thank Nathan Johnson-McDaniel for feedback on an earlier version of this work. This material is based upon work supported by the National Science Foundation under Grant No. 1417132. B. W. was supported by the John Templeton Foundation New Frontiers Program under Grant No. 37426 (University of Chicago)—FP050136-B (Cornell

University) and by the Irish Research Council, which is funded under the National Development Plan for Ireland. N. W. gratefully acknowledges support from a Marie Curie International Outgoing Fellowship (PIOF-GA-2012-627781) and the Irish Research Council, which is funded under the National Development Plan for Ireland. S. D. acknowledges support under EPSRC Grant No. EP/M025802/1, and from the Lancaster-Manchester-Sheffield Consortium for Fundamental Physics under STFC Grant No. ST/L000520/1. P. N. and A. C. O. acknowledge support from Science Foundation Ireland under Grant No. 10/RFP/PHY2847. C. K. is funded under the Programme for Research in Third Level Institutions (PRTLI) Cycle 5 and cofunded under the European Regional Development Fund.

APPENDIX A: GAUGE INVARIANTS IN SCHWARZSCHILD COORDINATES

In this Appendix we give explicit expressions for the perturbations to the octupolar invariants (as defined in Sec. II D 2) for the case of a circular orbit in Schwarzschild spacetime. Our expressions are written in terms of the components of h_{ab} and its partial derivatives in Schwarzschild coordinates, and are given by

$$\begin{aligned}\Delta\mathcal{E}_{111} = {}& \frac{h_{tt}M(8M-3r_0)(3M-2r_0)}{r_0^{5/2}(r_0-3M)^2(r_0-2M)^{3/2}} + \frac{h_{\phi\phi,r}M^2(13M-6r_0)}{2(3M-r_0)r_0^{11/2}(r_0-2M)^{1/2}} - \frac{2h_{r\phi,\phi r}M(r_0-2M)^{1/2}}{r_0^{9/2}} - \frac{2h_{tr,\phi r}M^{1/2}(r_0-2M)^{1/2}}{r_0^3} \\ & + \frac{h_{t\phi,rr}M^{1/2}(5M-2r_0)(r_0-2M)^{1/2}}{(3M-r_0)r_0^3} - \frac{h_{tt,rr}M(r_0-2M)^{1/2}}{(6M-2r_0)r_0^{3/2}} - \frac{2h_{r\phi,\phi}M(6M-r_0)(r_0-2M)^{1/2}}{r_0^{11/2}(r_0-3M)} \\ & - \frac{h_{\phi\phi,rr}M(11M-4r_0)(r_0-2M)^{1/2}}{2r_0^{9/2}(r_0-3M)} + \frac{h_{t\phi,rrr}M^{1/2}(r_0-2M)^{3/2}}{(3M-r_0)r_0^2} - \frac{h_{rr,r}M(6M-5r_0)(r_0-2M)^{3/2}}{2r_0^{9/2}(r_0-3M)} \\ & - \frac{h_{\phi\phi,rrr}M(r_0-2M)^{3/2}}{2r_0^{7/2}(r_0-3M)} - \frac{h_{tt,rrr}(r_0-2M)^{3/2}}{2r_0^{1/2}(r_0-3M)} + \frac{6h_{t\phi}M^{3/2}(r_0-2M)^{1/2}(4r_0-9M)}{r_0^5(r_0-3M)^2} \\ & + \frac{h_{tt,r}(-47M^2+42Mr_0-8r_0^2)}{2(3M-r_0)r_0^{5/2}(r_0-2M)^{1/2}} + \frac{h_{t\phi,r}M^{1/2}(-35M^2+30Mr_0-6r_0^2)}{(3M-r_0)r_0^4(r_0-2M)^{1/2}} + \frac{2h_{tr,\phi}M^{1/2}(12M^2-8Mr_0+r_0^2)}{r_0^4(r_0-3M)(r_0-2M)^{1/2}} \\ & + \frac{h_{\phi\phi}M(r_0-2M)^{1/2}(27M^2-18Mr_0+4r_0^2)}{r_0^{13/2}(r_0-3M)^2} - \frac{h_{rr}M(r_0-2M)^{1/2}(66M^2-73Mr_0+18r_0^2)}{2r_0^{11/2}(r_0-3M)},\end{aligned} \tag{A1}$$

$$\begin{aligned}\Delta\mathcal{E}_{122} = {}& -\frac{2h_{\theta\phi,\phi\theta}M}{3r_0^{11/2}(r_0-2M)^{1/2}} - \frac{2h_{t\theta,\phi\theta}M^{1/2}}{3r_0^4(r_0-2M)^{1/2}} + \frac{h_{tt,r}(14M-9r_0)}{6r_0^{5/2}(r_0-2M)^{1/2}} + \frac{h_{tt}M(20M-9r_0)}{3r_0^{5/2}(r_0-3M)^2(r_0-2M)^{1/2}} \\ & - \frac{2h_{t\phi,\theta\theta}M^{1/2}(7M-4r_0)}{3r_0^4(r_0-3M)(r_0-2M)^{1/2}} - \frac{5h_{\phi\phi,\theta\theta}M(r_0-2M)^{1/2}}{(9M-3r_0)r_0^{11/2}} + \frac{h_{\phi\phi,\theta r\theta}M(r_0-2M)^{1/2}}{(18M-6r_0)r_0^{9/2}} + \frac{h_{\phi\phi,\theta\theta r}M(r_0-2M)^{1/2}}{(9M-3r_0)r_0^{9/2}} \\ & + \frac{h_{tt,\theta r\theta}(r_0-2M)^{1/2}}{(18M-6r_0)r_0^{3/2}} + \frac{h_{tt,\theta\theta r}(r_0-2M)^{1/2}}{(9M-3r_0)r_0^{3/2}} - \frac{h_{\theta\theta}M(2M-5r_0)(r_0-2M)^{1/2}}{r_0^{13/2}(r_0-3M)} + \frac{h_{\theta\theta,r}M(6M-11r_0)(r_0-2M)^{1/2}}{6r_0^{11/2}(r_0-3M)} \\ & - \frac{h_{r\theta,\theta}M(6M-5r_0)(r_0-2M)^{1/2}}{3r_0^{11/2}(r_0-3M)} + \frac{2h_{r\phi,\phi}M(6M-r_0)(r_0-2M)^{1/2}}{3r_0^{11/2}(r_0-3M)} + \frac{2h_{tr,\phi}M^{1/2}(6M-r_0)(r_0-2M)^{1/2}}{3r_0^4(r_0-3M)} \\ & + \frac{h_{t\phi,rr}M^{1/2}(r_0-2M)^{3/2}}{(3M-r_0)r_0^3} - \frac{h_{\phi\phi,rr}M(r_0-2M)^{3/2}}{2r_0^{9/2}(r_0-3M)} - \frac{h_{tt,rr}(r_0-2M)^{3/2}}{2r_0^{3/2}(r_0-3M)} - \frac{h_{\phi\phi}M^2(r_0-2M)^{1/2}(18M+r_0)}{3r_0^{13/2}(r_0-3M)^2} \\ & + \frac{h_{tt,\theta\theta}(-4M+3r_0)}{3r_0^{5/2}(r_0-3M)(r_0-2M)^{1/2}} - \frac{h_{\phi\phi,r}M(6M^2+9Mr_0-5r_0^2)}{6(3M-r_0)r_0^{11/2}(r_0-2M)^{1/2}} + \frac{h_{t\phi,r}M^{1/2}(18M^2-25Mr_0+7r_0^2)}{3(3M-r_0)r_0^4(r_0-2M)^{1/2}} \\ & - \frac{2h_{t\phi}M^{3/2}(36M^2-38Mr_0+11r_0^2)}{3r_0^5(r_0-3M)^2(r_0-2M)^{1/2}} + \frac{h_{rr}M(r_0-2M)^{1/2}(36M^2-56Mr_0+19r_0^2)}{6r_0^{11/2}(r_0-3M)} + \frac{h_{t\phi,\theta r\theta}M^{1/2}(r_0-2M)^{1/2}}{9Mr_0^3-3r_0^4} \\ & + \frac{2h_{t\phi,\theta\theta r}M^{1/2}(r_0-2M)^{1/2}}{9Mr_0^3-3r_0^4},\end{aligned} \tag{A2}$$

$$\Delta\mathcal{E}_{133} = -\frac{h_{\phi\phi,\phi\phi}M(M-r_0)}{r_0^{11/2}(r_0-2M)^{3/2}} - \frac{2h_{t\phi,\phi\phi}M^{1/2}(M-r_0)}{r_0^4(r_0-2M)^{3/2}} - \frac{h_{\phi\phi,\phi r\phi}M}{6r_0^{9/2}(r_0-2M)^{1/2}} - \frac{h_{\phi\phi,\phi\phi r}M}{3r_0^{9/2}(r_0-2M)^{1/2}}$$
$$- \frac{h_{t\phi,\phi r\phi}M^{1/2}}{3r_0^3(r_0-2M)^{1/2}} - \frac{2h_{t\phi,\phi\phi r}M^{1/2}}{3r_0^3(r_0-2M)^{1/2}} + \frac{h_{tt,r}(23M-9r_0)}{6r_0^{5/2}(r_0-2M)^{1/2}} - \frac{h_{tt,\phi r\phi}}{6r_0^{3/2}(r_0-2M)^{1/2}}$$
$$- \frac{h_{tt,\phi\phi r}}{3r_0^{3/2}(r_0-2M)^{1/2}} - \frac{2h_{r\phi,\phi r}M(r_0-2M)^{1/2}}{3r_0^{9/2}} - \frac{2h_{tr,\phi r}M^{1/2}(r_0-2M)^{1/2}}{3r_0^3} + \frac{2h_{t\phi}M^{3/2}(M-r_0)(r_0-2M)^{1/2}}{r_0^5(r_0-3M)^2}$$
$$- \frac{h_{r\phi,\phi}M(30M-11r_0)(r_0-2M)^{1/2}}{3r_0^{11/2}(r_0-3M)} - \frac{h_{\phi\phi,rr}M(5M-r_0)(r_0-2M)^{1/2}}{6r_0^{9/2}(r_0-3M)} + \frac{h_{tt,rr}(7M-3r_0)(r_0-2M)^{1/2}}{6r_0^{3/2}(r_0-3M)}$$
$$- \frac{2h_{rr,r}M(r_0-2M)^{3/2}}{3r_0^{9/2}} + \frac{h_{tt,\phi\phi}(r_0-M)}{r_0^{5/2}(r_0-2M)^{3/2}} + \frac{h_{t\phi,rr}M^{1/2}(r_0-2M)^{1/2}(r_0-M)}{3(3M-r_0)r_0^3} + \frac{h_{tr,\phi}M^{1/2}(6M^2-7Mr_0+2r_0^2)}{3r_0^4(r_0-3M)(r_0-2M)^{1/2}}$$
$$+ \frac{h_{t\phi,r}M^{1/2}(63M^2-53Mr_0+11r_0^2)}{3(3M-r_0)r_0^4(r_0-2M)^{1/2}} + \frac{h_{\phi\phi,r}M(147M^2-125Mr_0+26r_0^2)}{6(3M-r_0)r_0^{11/2}(r_0-2M)^{1/2}}$$
$$+ \frac{h_{rr}M(r_0-2M)^{1/2}(150M^2-125Mr_0+27r_0^2)}{6r_0^{11/2}(r_0-3M)} - \frac{h_{tt}M(-66M^3+111M^2r_0-56Mr_0^2+9r_0^3)}{3r_0^{7/2}(r_0-3M)^2(r_0-2M)^{3/2}}$$
$$+ \frac{h_{\phi\phi}M(-222M^3+267M^2r_0-104Mr_0^2+13r_0^3)}{3r_0^{13/2}(r_0-3M)^2(r_0-2M)^{1/2}}, \tag{A3}$$

$$\Delta\mathcal{E}_{113} = \frac{h_{\phi\phi,\phi r}M(3M-r_0)}{3r_0^5(r_0-3M)^{1/2}(r_0-2M)^{1/2}} + \frac{4h_{t\phi,\phi r}M^{1/2}(3M-r_0)}{3r_0^{7/2}(r_0-3M)^{1/2}(r_0-2M)^{1/2}} + \frac{h_{tt,\phi r}(3M-r_0)}{r_0^2(r_0-3M)^{1/2}(r_0-2M)^{1/2}}$$
$$- \frac{2h_{r\phi,\phi\phi}M(r_0-3M)^{1/2}}{3r_0^5(r_0-2M)^{1/2}} - \frac{2h_{tr,\phi\phi}M^{1/2}(r_0-3M)^{1/2}}{3r_0^{7/2}(r_0-2M)^{1/2}} - \frac{h_{\phi\phi,\phi rr}M(r_0-2M)^{1/2}}{2r_0^4(r_0-3M)^{1/2}} - \frac{h_{t\phi,\phi rr}M^{1/2}(r_0-2M)^{1/2}}{r_0^{5/2}(r_0-3M)^{1/2}}$$
$$- \frac{h_{tt,\phi rr}(r_0-2M)^{1/2}}{2r_0(r_0-3M)^{1/2}} + \frac{h_{rr,\phi}M(r_0-2M)^{1/2}(-12M+7r_0)}{3r_0^5(r_0-3M)^{1/2}} + \frac{h_{\phi\phi,\phi}M(-15M^3+36M^2r_0-17Mr_0^2+2r_0^3)}{6r_0^6(r_0-3M)^{3/2}(r_0-2M)^{3/2}}$$
$$+ \frac{h_{tt,\phi}(-17M^3+32M^2r_0-15Mr_0^2+2r_0^3)}{2r_0^3(r_0-3M)^{3/2}(r_0-2M)^{3/2}} + \frac{h_{t\phi,\phi}M^{1/2}(-87M^3+120M^2r_0-49Mr_0^2+6r_0^3)}{3r_0^{9/2}(r_0-3M)^{3/2}(r_0-2M)^{3/2}}, \tag{A4}$$

$$\Delta\mathcal{E}_{223} = -\frac{h_{\phi\phi,\phi\theta\theta}M}{2r_0^5(r_0-3M)^{1/2}(r_0-2M)^{1/2}} + \frac{2h_{\phi\phi,\phi r}M^2}{3r_0^5(r_0-3M)^{1/2}(r_0-2M)^{1/2}} - \frac{4h_{t\theta,\theta}M^{3/2}}{3r_0^{9/2}(r_0-3M)^{1/2}(r_0-2M)^{1/2}}$$
$$- \frac{h_{t\phi,\phi\theta\theta}M^{1/2}}{r_0^{7/2}(r_0-3M)^{1/2}(r_0-2M)^{1/2}} + \frac{4h_{t\phi,\phi r}M^{3/2}}{3r_0^{7/2}(r_0-3M)^{1/2}(r_0-2M)^{1/2}} - \frac{h_{tt,\phi\theta\theta}}{2r_0^2(r_0-3M)^{1/2}(r_0-2M)^{1/2}}$$
$$+ \frac{2h_{tt,\phi r}M}{3r_0^2(r_0-3M)^{1/2}(r_0-2M)^{1/2}} - \frac{4h_{\theta\phi,\theta}M(r_0-2M)^{1/2}}{3r_0^6(r_0-3M)^{1/2}} + \frac{2h_{\theta\phi,\theta r}M(r_0-2M)^{1/2}}{3r_0^5(r_0-3M)^{1/2}} - \frac{2h_{r\phi,\theta\theta}M(r_0-2M)^{1/2}}{3r_0^5(r_0-3M)^{1/2}}$$
$$- \frac{4h_{r\phi}M(r_0-2M)^{1/2}}{3r_0^5(r_0-3M)^{1/2}} + \frac{2h_{t\theta,\theta r}M^{1/2}(r_0-2M)^{1/2}}{3r_0^{7/2}(r_0-3M)^{1/2}} - \frac{2h_{tr,\theta\theta}M^{1/2}(r_0-2M)^{1/2}}{3r_0^{7/2}(r_0-3M)^{1/2}} - \frac{h_{\theta\theta,\phi}M(6M+r_0)}{3r_0^6(r_0-3M)^{1/2}(r_0-2M)^{1/2}}$$
$$+ \frac{h_{tt,\phi}(-6M^3-11M^2r_0+14Mr_0^2-3r_0^3)}{6r_0^3(r_0-3M)^{3/2}(r_0-2M)^{3/2}} - \frac{h_{\phi\phi,\phi}M(6M^3+11M^2r_0-14Mr_0^2+3r_0^3)}{6r_0^6(r_0-3M)^{3/2}(r_0-2M)^{3/2}}$$
$$- \frac{h_{t\phi,\phi}M^{1/2}(6M^3+11M^2r_0-14Mr_0^2+3r_0^3)}{3r_0^{9/2}(r_0-3M)^{3/2}(r_0-2M)^{3/2}}, \tag{A5}$$

$$\Delta\mathcal{E}_{333} = -\frac{h_{\phi\phi,\phi\phi\phi}M(r_0-3M)^{1/2}}{2r_0^5(r_0-2M)^{3/2}} - \frac{h_{t\phi,\phi\phi\phi}M^{1/2}(r_0-3M)^{1/2}}{r_0^{7/2}(r_0-2M)^{3/2}} - \frac{h_{tt,\phi\phi\phi}(r_0-3M)^{1/2}}{2r_0^2(r_0-2M)^{3/2}} - \frac{h_{tt,\phi}(r_0-3M)^{3/2}}{2r_0^3(r_0-2M)^{3/2}}$$
$$+ \frac{h_{\phi\phi,\phi}M(7M-5r_0)(3M-r_0)}{2(2M-r_0)r_0^6(r_0-3M)^{1/2}(r_0-2M)^{1/2}} + \frac{2h_{\phi\phi,\phi r}M(r_0-3M)^{1/2}}{r_0^5(r_0-2M)^{1/2}} - \frac{2h_{r\phi,\phi\phi}M(r_0-3M)^{1/2}}{r_0^5(r_0-2M)^{1/2}}$$
$$+ \frac{2h_{t\phi,\phi r}M^{1/2}(r_0-3M)^{1/2}}{r_0^{7/2}(r_0-2M)^{1/2}} - \frac{2h_{tr,\phi\phi}M^{1/2}(r_0-3M)^{1/2}}{r_0^{7/2}(r_0-2M)^{1/2}} - \frac{2h_{rr,\phi}M(r_0-3M)^{1/2}(r_0-2M)^{1/2}}{r_0^5}$$
$$+ \frac{h_{t\phi,\phi}M^{1/2}(3M-r_0)(M+r_0)}{r_0^{9/2}(r_0-3M)^{1/2}(r_0-2M)^{3/2}}, \tag{A6}$$

$$\Delta\mathcal{B}_{123} = \frac{h_{tr,\theta\theta}(7M-2r_0)(2M-r_0)}{3r_0^{7/2}(r_0-3M)^{3/2}} + \frac{h_{\theta\phi,\theta}M^{3/2}}{3r_0^6(r_0-3M)^{1/2}} - \frac{h_{\theta\phi,\theta r}M^{3/2}}{6r_0^5(r_0-3M)^{1/2}} + \frac{h_{r\phi,\theta\theta}M^{3/2}}{6r_0^5(r_0-3M)^{1/2}}$$
$$- \frac{h_{\theta\phi,\phi\phi\theta}M^{3/2}}{6(2M-r_0)r_0^5(r_0-3M)^{1/2}} - \frac{h_{\theta\theta,\phi\phi\phi}M^{3/2}}{6(2M-r_0)r_0^5(r_0-3M)^{1/2}} + \frac{h_{rr,\phi\theta\theta}M^{1/2}(2M-r_0)}{6r_0^4(r_0-3M)^{1/2}}$$
$$- \frac{h_{t\phi,\phi\theta\theta}M}{(12M-6r_0)r_0^{7/2}(r_0-3M)^{1/2}} - \frac{h_{t\theta,\phi\phi\theta}M}{(4M-2r_0)r_0^{7/2}(r_0-3M)^{1/2}} + \frac{h_{tr,\theta\theta r}(2M-r_0)}{3r_0^{5/2}(r_0-3M)^{1/2}}$$
$$- \frac{h_{tt,\phi\theta\theta}M^{1/2}}{3(2M-r_0)r_0^2(r_0-3M)^{1/2}} - \frac{h_{t\phi,\theta\theta}}{6r_0^{3/2}(r_0-3M)^{1/2}} - \frac{h_{tt,\phi rr}M^{1/2}}{3r_0(r_0-3M)^{1/2}} + \frac{h_{tr,\phi\phi r}(r_0-4M)}{6r_0^{5/2}(r_0-3M)^{1/2}}$$
$$+ \frac{h_{\theta\theta,\phi rr}M^{1/2}(r_0-2M)}{6r_0^4(r_0-3M)^{1/2}} + \frac{h_{rr,\phi\phi\phi}M^{1/2}(r_0-2M)}{6r_0^4(r_0-3M)^{1/2}} + \frac{h_{t\theta,\theta rr}(r_0-2M)}{3r_0^{5/2}(r_0-3M)^{1/2}}$$
$$+ \frac{h_{rr,\phi r}M^{1/2}(r_0-3M)^{1/2}(r_0-2M)}{6(3M-r_0)r_0^3} - \frac{h_{r\theta,\phi\theta}M^{1/2}(-13M^2+17Mr_0-4r_0^2)}{6r_0^5(r_0-3M)^{3/2}}$$
$$+ \frac{h_{\theta\theta,\phi r}M^{1/2}(-8M^2+9Mr_0-2r_0^2)}{3r_0^5(r_0-3M)^{3/2}} + \frac{h_{t\theta,\theta r}(-8M^2+9Mr_0-2r_0^2)}{3r_0^{7/2}(r_0-3M)^{3/2}} + \frac{2h_{t\phi,\phi}M(M^2+4Mr_0-r_0^2)}{3(2M-r_0)r_0^{9/2}(r_0-3M)^{3/2}}$$
$$+ \frac{h_{\phi\phi,\phi r}M^{1/2}(32M^2-13Mr_0+r_0^2)}{6r_0^5(r_0-3M)^{3/2}} - \frac{2h_{t\theta,\theta}M(20M^2-19Mr_0+4r_0^2)}{3(2M-r_0)r_0^{9/2}(r_0-3M)^{3/2}} - \frac{h_{r\phi}M(3M^{3/2}r_0^{3/2}-M^{1/2}r_0^{5/2})}{3r_0^{13/2}(r_0-3M)^{3/2}}$$
$$+ \frac{2h_{tt,\phi r}M^{1/2}(r_0-3M)^{1/2}}{6Mr_0^2-3r_0^3} - \frac{h_{r\phi,\phi\phi}M^{1/2}(28M^3-37M^2r_0+15Mr_0^2-2r_0^3)}{6(2M-r_0)r_0^5(r_0-3M)^{3/2}}$$
$$+ \frac{h_{tr,\phi\phi}(52M^3-57M^2r_0+19Mr_0^2-2r_0^3)}{6r_0^{7/2}(r_0-3M)^{3/2}(r_0-2M)} - \frac{h_{\phi\phi,\phi}M^{1/2}(26M^3-36M^2r_0+11Mr_0^2-r_0^3)}{6(2M-r_0)r_0^6(r_0-3M)^{3/2}}$$
$$- \frac{h_{t\phi,\phi r}(-100M^3+91M^2r_0-25Mr_0^2+2r_0^3)}{6(2M-r_0)r_0^{7/2}(r_0-3M)^{3/2}} - \frac{h_{\theta\theta,\phi}M^{1/2}(4M^3+7M^2r_0-9Mr_0^2+2r_0^3)}{3(2M-r_0)r_0^6(r_0-3M)^{3/2}}$$
$$+ \frac{h_{rr,\phi}(68M^{7/2}r_0^{1/2}-45M^{5/2}r_0^{3/2}+4M^{3/2}r_0^{5/2}+M^{1/2}r_0^{7/2})}{6r_0^{11/2}(r_0-3M)^{3/2}}$$
$$+ \frac{h_{tt,\phi}(-72M^{7/2}r_0^{1/2}+109M^{5/2}r_0^{3/2}-47M^{3/2}r_0^{5/2}+6M^{1/2}r_0^{7/2})}{6r_0^{7/2}(r_0-3M)^{3/2}(r_0-2M)^2} + \frac{h_{r\phi,\phi\phi r}M^{1/2}(r_0-3M)^{1/2}}{18Mr_0^3-6r_0^4}, \tag{A7}$$

$$\Delta\mathcal{B}_{211} = -\frac{h_{r\theta,\phi\phi\theta}M^{1/2}}{6r_0^{9/2}} + \frac{h_{rr,\phi\phi}M^{1/2}(4M-3r_0)}{6r_0^{9/2}} - \frac{h_{tr,\phi\theta\theta}M}{6(3M-r_0)r_0^3} - \frac{2h_{tt,\theta\theta r}M^{1/2}}{(9M-3r_0)r_0^{3/2}} + \frac{h_{t\theta,\phi\theta r}(r_0-8M)}{6(3M-r_0)r_0^3}$$
$$+ \frac{6h_{\theta\theta}M^{3/2}(2M-r_0)}{r_0^{13/2}(r_0-3M)} - \frac{10h_{\theta\theta,r}M^{3/2}(2M-r_0)}{3r_0^{11/2}(r_0-3M)} + \frac{16h_{r\theta,\theta}M^{3/2}(2M-r_0)}{3r_0^{11/2}(r_0-3M)} + \frac{h_{\theta\phi,\phi\theta r}M^{3/2}}{6r_0^{9/2}(r_0-3M)} + \frac{h_{\theta\theta,\phi\phi r}M^{3/2}}{3r_0^{9/2}(r_0-3M)}$$
$$+ \frac{h_{\theta\theta,rr}M^{3/2}(2M-r_0)}{3r_0^{9/2}(r_0-3M)} - \frac{2h_{r\theta,\theta r}M^{3/2}(2M-r_0)}{3r_0^{9/2}(r_0-3M)} + \frac{h_{rr,r}M^{3/2}(22M-9r_0)(2M-r_0)}{3r_0^{9/2}(r_0-3M)}$$
$$+ \frac{h_{r\phi,\phi r}M^{1/2}(M-r_0)(4M-r_0)}{6r_0^{9/2}(r_0-3M)} - \frac{h_{\theta\phi,\phi\theta}M^{1/2}(M-r_0)^2}{6r_0^{11/2}(r_0-3M)(r_0-2M)} + \frac{h_{tt,\theta\theta}M^{1/2}(5M-4r_0)}{3r_0^{5/2}(r_0-3M)(r_0-2M)} + \frac{h_{tr,\phi rr}(r_0-2M)}{3r_0^2}$$
$$+ \frac{h_{tt,rrr}M^{1/2}(r_0-2M)}{(9M-3r_0)r_0^{1/2}} + \frac{h_{r\phi,\phi\theta\theta}M^{1/2}(r_0-2M)}{6r_0^{9/2}(r_0-3M)} + \frac{h_{rr,\theta\theta}M^{3/2}(r_0-2M)}{3r_0^{9/2}(r_0-3M)} + \frac{h_{rr,\phi\phi r}M^{1/2}(r_0-2M)^2}{3r_0^{7/2}(r_0-3M)}$$
$$- \frac{h_{rr,rr}M^{3/2}(r_0-2M)^2}{3r_0^{7/2}(r_0-3M)} + \frac{4h_{\phi\phi}M^{3/2}(r_0-2M)(r_0-M)}{r_0^{13/2}(r_0-3M)^2} + \frac{h_{tt,rr}M^{1/2}(-3M+2r_0)}{3r_0^{3/2}(r_0-3M)} + \frac{4h_{\phi\phi,r}M^{3/2}(-8M+3r_0)}{3r_0^{11/2}(r_0-3M)}$$
$$+ \frac{h_{t\phi,\theta\theta}(-9M^2+10Mr_0-3r_0^2)}{6r_0^4(r_0-3M)(r_0-2M)} + \frac{h_{\theta\theta,\phi\phi}M^{1/2}(10M^2-9Mr_0+r_0^2)}{6r_0^{11/2}(r_0-3M)(r_0-2M)} - \frac{h_{r\phi,\phi rr}M^{1/2}(2M^2-3Mr_0+r_0^2)}{3r_0^{7/2}(r_0-3M)}$$
$$+ \frac{h_{t\theta,\phi\theta}(31M^2-26Mr_0+3r_0^2)}{6r_0^4(r_0-3M)(r_0-2M)} + \frac{h_{r\phi,\phi}M^{1/2}(16M^2-21Mr_0+4r_0^2)}{6r_0^{11/2}(r_0-3M)} + \frac{h_{tt,r}M^{1/2}(70M^2-57Mr_0+10r_0^2)}{3r_0^{5/2}(r_0-3M)(r_0-2M)}$$
$$- \frac{2h_{rr}M^{3/2}(94M^2-83Mr_0+18r_0^2)}{3r_0^{11/2}(r_0-3M)} + \frac{h_{t\phi,rrr}(2M^2-3Mr_0+r_0^2)}{9Mr_0^2-3r_0^3} + \frac{h_{tr,\phi}(-112M^3+156M^2r_0-61Mr_0^2+6r_0^3)}{6r_0^4(r_0-3M)(r_0-2M)}$$
$$+ \frac{2h_{tt}M^{3/2}(-114M^3+189M^2r_0-103Mr_0^2+18r_0^3)}{3r_0^{7/2}(r_0-3M)^2(r_0-2M)^2} + \frac{h_{t\phi}M(-120M^3+239M^2r_0-145Mr_0^2+28r_0^3)}{3r_0^5(r_0-3M)^2(r_0-2M)}$$
$$+ \frac{h_{t\phi,\theta\theta r}(M-r_0)}{18Mr_0^3-6r_0^4} + \frac{h_{tr,\phi r}(36M^2-29Mr_0+5r_0^2)}{18Mr_0^3-6r_0^4} - \frac{h_{t\phi,rr}(12M^2-17Mr_0+5r_0^2)}{18Mr_0^3-6r_0^4}$$
$$+ \frac{h_{t\phi,r}(136M^2-63Mr_0+6r_0^2)}{18Mr_0^4-6r_0^5}, \tag{A8}$$

$$\Delta\mathcal{B}_{222} = -\frac{h_{\theta\theta,\phi\phi}M^{1/2}}{2r_0^{11/2}} + \frac{h_{r\theta,\phi\phi\theta}M^{1/2}}{2r_0^{9/2}} + \frac{h_{r\phi,\phi\theta\theta}M^{3/2}}{(6M-2r_0)r_0^{9/2}} - \frac{h_{t\phi,\theta\theta}}{(3M-r_0)r_0^3} + \frac{h_{tt,\theta\theta r}M^{1/2}}{(3M-r_0)r_0^{3/2}} + \frac{h_{t\theta,\phi\theta}(r_0-5M)}{(3M-r_0)r_0^4}$$
$$- \frac{8h_{\theta\theta}M^{3/2}(2M-r_0)}{r_0^{13/2}(r_0-3M)} + \frac{h_{\phi\phi,r}M^{3/2}(8M-3r_0)}{r_0^{11/2}(r_0-3M)} + \frac{4h_{\theta\theta,r}M^{3/2}(2M-r_0)}{r_0^{11/2}(r_0-3M)} - \frac{8h_{r\theta,\theta}M^{3/2}(2M-r_0)}{r_0^{11/2}(r_0-3M)}$$
$$+ \frac{h_{rr}M^{3/2}(20M-9r_0)(2M-r_0)}{r_0^{11/2}(r_0-3M)} + \frac{h_{\theta\phi,\phi\theta r}M^{1/2}(2M-r_0)}{2r_0^{9/2}(r_0-3M)} + \frac{h_{rr,\theta\theta}M^{3/2}(2M-r_0)}{r_0^{9/2}(r_0-3M)} + \frac{h_{tt,r}M^{1/2}(7M-2r_0)}{r_0^{5/2}(r_0-3M)}$$
$$+ \frac{h_{tt,rr}M^{1/2}(2M-r_0)}{r_0^{3/2}(r_0-3M)} + \frac{h_{rr,\phi\phi}M^{1/2}(r_0-2M)}{2r_0^{9/2}} + \frac{h_{r\phi,\phi}M^{1/2}(r_0-2M)}{2r_0^{9/2}(r_0-3M)} - \frac{h_{rr,r}M^{3/2}(r_0-2M)^2}{r_0^{9/2}(r_0-3M)}$$
$$+ \frac{h_{\theta\phi,\phi\theta}M^{1/2}(r_0-M)}{r_0^{11/2}(r_0-3M)} - \frac{3h_{\phi\phi}M^{3/2}(r_0-2M)(r_0-M)}{r_0^{13/2}(r_0-3M)^2} + \frac{h_{tt,\theta\theta}M^{1/2}(2r_0-3M)}{r_0^{5/2}(r_0-3M)(r_0-2M)}$$
$$+ \frac{h_{tt}M^{3/2}(-36M^2+37Mr_0-9r_0^2)}{r_0^{7/2}(r_0-3M)^2(r_0-2M)} + \frac{h_{t\phi}M(-6M^2+7Mr_0-3r_0^2)}{r_0^5(r_0-3M)^2} - \frac{h_{r\phi,\phi r}M^{1/2}(2M^2-3Mr_0+r_0^2)}{2r_0^{9/2}(r_0-3M)}$$
$$+ \frac{h_{t\theta,\phi\theta r}M}{6Mr_0^3-2r_0^4} - \frac{h_{t\phi,\theta\theta r}(M-r_0)}{6Mr_0^3-2r_0^4} + \frac{h_{tr,\phi\theta\theta}(4M-r_0)}{6Mr_0^3-2r_0^4} - \frac{h_{tr,\phi r}(10M^2-7Mr_0+r_0^2)}{6Mr_0^3-2r_0^4} + \frac{h_{t\phi,rr}(2M^2-3Mr_0+r_0^2)}{6Mr_0^3-2r_0^4}$$
$$- \frac{h_{t\phi,r}(36M^2-16Mr_0+r_0^2)}{6Mr_0^4-2r_0^5} + \frac{h_{tr,\phi}(18M^2-10Mr_0+r_0^2)}{6Mr_0^4-2r_0^5}, \tag{A9}$$

$$\Delta\mathcal{B}_{233} = \frac{h_{\theta\phi,\phi\theta r}M^{1/2}}{6r_0^{9/2}} - \frac{h_{r\phi,\phi\theta\theta}M^{1/2}}{6r_0^{9/2}} + \frac{h_{\theta\theta,\phi\phi r}M^{1/2}}{3r_0^{9/2}} - \frac{h_{r\theta,\phi\phi\theta}M^{1/2}}{3r_0^{9/2}} + \frac{h_{r\phi,\phi\phi\phi}M^{3/2}}{(6M-3r_0)r_0^{9/2}} + \frac{h_{r\phi,\phi r}M^{5/2}}{(9M-3r_0)r_0^{9/2}} - \frac{h_{rr,\phi\phi}M^{1/2}}{3r_0^{7/2}}$$
$$+ \frac{h_{t\theta,r\theta\phi}}{2r_0^3} - \frac{h_{tr,\phi\theta\theta}}{2r_0^3} + \frac{h_{tt,\phi\phi r}M^{1/2}}{(6M-3r_0)r_0^{3/2}} - \frac{2h_{\theta\theta}M^{3/2}(2M-r_0)}{3r_0^{13/2}(r_0-3M)} + \frac{h_{\phi\phi,\phi\phi}M^{3/2}}{3r_0^{11/2}(r_0-3M)} + \frac{h_{\phi\phi,r}M^{3/2}(16M-7r_0)}{3r_0^{11/2}(r_0-3M)}$$
$$+ \frac{2h_{\theta\theta,r}M^{3/2}(2M-r_0)}{3r_0^{11/2}(r_0-3M)} + \frac{h_{rr}M^{3/2}(22M-9r_0)(2M-r_0)}{3r_0^{11/2}(r_0-3M)} + \frac{2h_{r\theta,\theta r}M^{3/2}(2M-r_0)}{3r_0^{9/2}(r_0-3M)} + \frac{2h_{tt,r}M^{1/2}(4M-r_0)}{3r_0^{5/2}(r_0-3M)}$$
$$+ \frac{h_{tt,rr}M^{1/2}(2M-r_0)}{3r_0^{3/2}(r_0-3M)} + \frac{2h_{\theta\theta,\phi\phi}M^{1/2}(M-r_0)}{3r_0^{11/2}(r_0-2M)} - \frac{2h_{t\phi,\phi\phi}M(5M-2r_0)}{3r_0^4(r_0-3M)(r_0-2M)} + \frac{h_{tt,\theta\theta}M^{3/2}}{3r_0^{5/2}(r_0-3M)(r_0-2M)}$$
$$+ \frac{h_{\theta\theta,rr}M^{3/2}(r_0-2M)}{3r_0^{9/2}(r_0-3M)} + \frac{h_{rr,\theta\theta}M^{3/2}(r_0-2M)}{3r_0^{9/2}(r_0-3M)} - \frac{2h_{rr,r}M^{3/2}(r_0-2M)^2}{3r_0^{9/2}(r_0-3M)} + \frac{h_{tr,\phi r}M(2r_0-5M)}{3(3M-r_0)r_0^3}$$
$$+ \frac{h_{\phi\phi}M^{3/2}(r_0-2M)(5r_0-21M)}{3r_0^{13/2}(r_0-3M)^2} + \frac{h_{t\theta,\phi\theta}(5M^2+8Mr_0-3r_0^2)}{6r_0^4(r_0-3M)(r_0-2M)} + \frac{h_{\theta\phi,\phi\theta}M^{1/2}(5M^2-4Mr_0+r_0^2)}{6r_0^{11/2}(r_0-3M)(r_0-2M)}$$
$$+ \frac{h_{r\phi,\phi}M^{1/2}(-32M^2+11Mr_0+r_0^2)}{6r_0^{11/2}(r_0-3M)} + \frac{h_{tt,\phi\phi}M^{1/2}(7M^2-8Mr_0+2r_0^2)}{3r_0^{5/2}(r_0-3M)(r_0-2M)^2} + \frac{h_{t\phi,\theta\theta}(17M^2-14Mr_0+3r_0^2)}{6r_0^4(r_0-3M)(r_0-2M)}$$
$$- \frac{h_{tt}M^{3/2}(30M^2-35Mr_0+9r_0^2)}{3r_0^{7/2}(r_0-3M)^2(r_0-2M)} + \frac{h_{tr,\phi}(28M^3-42M^2r_0+21Mr_0^2-3r_0^3)}{6r_0^4(r_0-3M)(r_0-2M)}$$
$$+ \frac{h_{t\phi}M(-12M^3+23M^2r_0-14Mr_0^2+3r_0^3)}{3(2M-r_0)r_0^5(r_0-3M)^2} + \frac{h_{t\phi,\phi\phi r}M}{6Mr_0^3-3r_0^4} + \frac{h_{tr,\phi\phi\phi}M}{6Mr_0^3-3r_0^4} + \frac{h_{t\phi,rr}M^2}{9Mr_0^3-3r_0^4}$$
$$- \frac{h_{t\phi,r}(36M^2-23Mr_0+3r_0^2)}{18Mr_0^4-6r_0^5}. \tag{A10}$$

APPENDIX B: SHIFT TO ASYMPTOTICALLY FLAT GAUGE

In order to compare our results with PN theory it is necessary to work in an asymptotically flat gauge. In both the Lorenz and Zerilli gauges the *tt*-component of the metric perturbation does not vanish at spatial infinity and so we make an $\mathcal{O}(\mu)$ gauge transformation to correct for this [32]. For both gauges this correction can be made by adding $h^{NAF}_{ab} = \xi_{a;b} + \xi_{b;a}$ where $\xi^a = [-\alpha(t + r_* - r), 0, 0, 0]$ and $\alpha = \mu/\sqrt{r_0(r_0 - 3M)}$. Explicitly, this can be achieved by adding an extra term to the invariants, $\Delta\mathcal{E}_{ijk} \to \Delta\mathcal{E}_{ijk} + \delta^\xi\mathcal{E}_{ijk}$ and $\Delta\mathcal{B}_{ijk} \to \Delta\mathcal{B}_{ijk} + \delta^\xi\mathcal{B}_{ijk}$ where

$$\delta^\xi\mathcal{E}_{111} = \frac{2\alpha M(-81M^3+111M^2r_0-51Mr_0^2+8r_0^3)}{r_0^{9/2}(r_0-3M)^2(r_0-2M)^{1/2}}, \tag{B1a}$$

$$\delta^\xi\mathcal{E}_{122} = \frac{2\alpha M(54M^3-109M^2r_0+64Mr_0^2-12r_0^3)}{3r_0^{9/2}(r_0-3M)^2(r_0-2M)^{1/2}}, \tag{B1b}$$

$$\delta^\xi\mathcal{E}_{133} = \frac{2\alpha M(189M^3-224M^2r_0+89Mr_0^2-12r_0^3)}{3r_0^{9/2}(r_0-3M)^2(r_0-2M)^{1/2}}, \tag{B1c}$$

$$\delta^\xi\mathcal{E}_{113} = 0, \tag{B1d}$$

$$\delta^\xi\mathcal{E}_{223} = 0, \tag{B1e}$$

$$\delta^\xi\mathcal{E}_{333} = 0, \tag{B1f}$$

$$\delta^\xi\mathcal{B}_{123} = 0, \tag{B1g}$$

$$\delta^\xi\mathcal{B}_{211} = \frac{8\alpha M^{3/2}(54M^2-43Mr_0+9r_0^2)}{3r_0^{9/2}(r_0-3M)^2}, \tag{B1h}$$

$$\delta^\xi\mathcal{B}_{222} = -\frac{2\alpha M^{3/2}(54M^2-43Mr_0+9r_0^2)}{r_0^{9/2}(r_0-3M)^2}, \tag{B1i}$$

$$\delta^\xi\mathcal{B}_{233} = -\frac{2\alpha M^{3/2}(54M^2-43Mr_0+9r_0^2)}{3r_0^{9/2}(r_0-3M)^2}. \tag{B1j}$$

[1] F. Pretorius, Phys. Rev. Lett. **95**, 121101 (2005).
[2] B. Bruegmann, J. A. Gonzalez, M. Hannam, S. Husa, and U. Sperhake, Phys. Rev. D **77**, 124047 (2008).
[3] C. M. Will, Proc. Natl. Acad. Sci. U.S.A. **108**, 5938 (2011).
[4] T. Hinderer, A. Buonanno, A. H. Mroué, D. A. Hemberger, G. Lovelace *et al.*, Phys. Rev. D **88**, 084005 (2013).
[5] J. Aasi *et al.* (LIGO Scientific), Classical Quantum Gravity **32**, 074001 (2015).
[6] S. Bernuzzi, A. Nagar, T. Dietrich, and T. Damour, Phys. Rev. Lett. **114**, 161103 (2015).
[7] P. Landry and E. Poisson, Phys. Rev. D **91**, 104026 (2015).
[8] P. Schmidt, M. Hannam, and S. Husa, Phys. Rev. D **86**, 104063 (2012).
[9] M. Hannam, P. Schmidt, A. Bohé, L. Haegel, S. Husa, F. Ohme, G. Pratten, and M. Pürrer, Phys. Rev. Lett. **113**, 151101 (2014).
[10] P. Schmidt, F. Ohme, and M. Hannam, Phys. Rev. D **91**, 024043 (2015).
[11] S. E. Field, C. R. Galley, J. S. Hesthaven, J. Kaye, and M. Tiglio, Phys. Rev. X **4**, 031006 (2014).
[12] R. H. Cole and J. R. Gair, Phys. Rev. D **90**, 124043 (2014).
[13] J. Blackman, S. E. Field, C. R. Galley, B. Szilágyi, M. A. Scheel, M. Tiglio, and D. A. Hemberger, Phys. Rev. Lett. **115**, 121102 (2015).
[14] C. J. Moore and J. R. Gair, Phys. Rev. Lett. **113**, 251101 (2014).
[15] A. Buonanno and T. Damour, Phys. Rev. D **59**, 084006 (1999).
[16] T. Damour, A. Nagar, and S. Bernuzzi, Phys. Rev. D **87**, 084035 (2013).
[17] A. Taracchini, A. Buonanno, Y. Pan, T. Hinderer, M. Boyle *et al.*, Phys. Rev. D **89**, 061502 (2014).
[18] T. Damour, arXiv:1312.3505.
[19] T. Damour, P. Jaranowski, and G. Schäfer, Phys. Rev. D **91**, 084024 (2015).
[20] E. Poisson, A. Pound, and I. Vega, Living Rev. Relativity **14**, 7 (2011).
[21] L. Barack, Classical Quantum Gravity **26**, 213001 (2009).
[22] J. Thornburg, GW Notes **5**, 3 (2011).
[23] T. Damour, Phys. Rev. D **81**, 024017 (2010).
[24] L. Barack, T. Damour, and N. Sago, Phys. Rev. D **82**, 084036 (2010).
[25] S. Akcay, L. Barack, T. Damour, and N. Sago, Phys. Rev. D **86**, 104041 (2012).
[26] D. Bini and T. Damour, Phys. Rev. D **90**, 024039 (2014).
[27] D. Bini and T. Damour, Phys. Rev. D **90**, 124037 (2014).
[28] Y. Mino, M. Sasaki, and T. Tanaka, Phys. Rev. D **55**, 3457 (1997).
[29] T. C. Quinn and R. M. Wald, Phys. Rev. D **56**, 3381 (1997).
[30] A. Le Tiec, Int. J. Mod. Phys. D **23**, 1430022 (2014).
[31] S. L. Detweiler, Phys. Rev. D **77**, 124026 (2008).
[32] N. Sago, L. Barack, and S. L. Detweiler, Phys. Rev. D **78**, 124024 (2008).
[33] L. Barack and N. Sago, Phys. Rev. Lett. **102**, 191101 (2009).
[34] L. Barack and N. Sago, Phys. Rev. D **83**, 084023 (2011).
[35] S. R. Dolan, N. Warburton, A. I. Harte, A. Le Tiec, B. Wardell, and L. Barack, Phys. Rev. D **89**, 064011 (2014).
[36] D. Bini and T. Damour, Phys. Rev. D **91**, 064064 (2015).
[37] S. R. Dolan, P. Nolan, A. C. Ottewill, N. Warburton, and B. Wardell, Phys. Rev. D **91**, 023009 (2015).
[38] D. Bini and A. Geralico, Phys. Rev. D **91**, 084012 (2015).
[39] S. Akcay, A. Le Tiec, L. Barack, N. Sago, and N. Warburton, Phys. Rev. D **91**, 124014 (2015).
[40] S. Isoyama, L. Barack, S. R. Dolan, A. Le Tiec, H. Nakano, A. G. Shah, T. Tanaka, and N. Warburton, Phys. Rev. Lett. **113**, 161101 (2014).
[41] N. K. Johnson-McDaniel, A. G. Shah, and B. F. Whiting, Phys. Rev. D **92**, 044007 (2015).
[42] A. G. Shah and A. Pound, Phys. Rev. D **91**, 124022 (2015).
[43] C. Kavanagh, A. C. Ottewill, and B. Wardell, Phys. Rev. D **92**, 084025 (2015).
[44] D. H. Bailey, J. M. Borwein, D. Broadhurst, and W. Zudilin, Contemp. Math. **517**, 41 (2010).
[45] N. K. Johnson-McDaniel, N. Yunes, W. Tichy, and B. J. Owen, Phys. Rev. D **80**, 124039 (2009).
[46] M. Ishii, M. Shibata, and Y. Mino, Phys. Rev. D **71**, 044017 (2005).
[47] E. Poisson and I. Vlasov, Phys. Rev. D **81**, 024029 (2010).
[48] B. C. Mundim, H. Nakano, N. Yunes, M. Campanelli, S. C. Noble, and Y. Zlochower, Phys. Rev. D **89**, 084008 (2014).
[49] Y. Zlochower, H. Nakano, B. C. Mundim, M. Campanelli, S. Noble *et al.*, arXiv:1504.00286
[50] S. L. Detweiler and B. F. Whiting, Phys. Rev. D **67**, 024025 (2003).
[51] A. I. Harte, Classical Quantum Gravity **29**, 055012 (2012).
[52] J.-A. Marck, Proc. R. Soc. A **385**, 431 (1983).
[53] A. G. Shah, J. L. Friedman, and T. S. Keidl, Phys. Rev. D **86**, 084059 (2012).
[54] T. Regge and J. A. Wheeler, Phys. Rev. **108**, 1063 (1957).
[55] F. J. Zerilli, Phys. Rev. D **2**, 2141 (1970).
[56] M. V. Berndtson, Ph.D. thesis, Colorado U., 2007 [arXiv:0904.0033].
[57] S. Hopper and C. R. Evans, Phys. Rev. D **82**, 084010 (2010).
[58] F. J. Zerilli, Phys. Rev. D **2**, 2141 (1970).
[59] S. Detweiler and E. Poisson, Phys. Rev. D **69**, 084019 (2004).
[60] S. Akcay, Phys. Rev. D **83**, 124026 (2011).
[61] B. Wardell and N. Warburton, Phys. Rev. D **92**, 084019 (2015).
[62] S. Akcay, N. Warburton, and L. Barack, Phys. Rev. D **88**, 104009 (2013).
[63] D. Bini and T. Damour, Phys. Rev. D **89**, 064063 (2014).
[64] A. G. Shah, J. L. Friedman, and B. F. Whiting, Phys. Rev. D **89**, 064042 (2014).
[65] A. G. Shah, Phys. Rev. D **90**, 044025 (2014).
[66] Electronic archive of post-Newtonian coefficients, http://www.barrywardell.net/research/code.
[67] D. Bini, T. Damour, and G. Faye, Phys. Rev. D **85**, 124034 (2012).
[68] F. K. Manasse, J. Math. Phys. (N.Y.) **4**, 746 (1963).
[69] K. S. Thorne and J. B. Hartle, Phys. Rev. D **31**, 1815 (1985).
[70] K. Alvi, Phys. Rev. D **61**, 124013 (2000).
[71] S. L. Detweiler, Phys. Rev. Lett. **86**, 1931 (2001).
[72] S. L. Detweiler, Classical Quantum Gravity **22**, S681 (2005).
[73] E. Poisson, Phys. Rev. Lett. **94**, 161103 (2005).
[74] S. Taylor and E. Poisson, Phys. Rev. D **78**, 084016 (2008).

[75] E. Poisson, Phys. Rev. D **91**, 044004 (2015).
[76] A. Pound, Phys. Rev. D **81**, 124009 (2010).
[77] N. Yunes, W. Tichy, B. J. Owen, and B. Bruegmann, Phys. Rev. D **74**, 104011 (2006).
[78] N. Yunes and W. Tichy, Phys. Rev. D **74**, 064013 (2006).
[79] L. Gallouin, H. Nakano, N. Yunes, and M. Campanelli, Classical Quantum Gravity **29**, 235013 (2012).
[80] T. Chu, Phys. Rev. D **89**, 064062 (2014).
[81] A. Pound, Phys. Rev. Lett. **109**, 051101 (2012).
[82] S. E. Gralla, Phys. Rev. D **85**, 124011 (2012).
[83] S. Detweiler, Phys. Rev. D **85**, 044048 (2012).
[84] A. Pound and J. Miller, Phys. Rev. D **89**, 104020 (2014).
[85] N. Warburton and B. Wardell, Phys. Rev. D **89**, 044046 (2014).
[86] A. Pound, Phys. Rev. D **90**, 084039 (2014).